Developmental Biology 495 (2023) 21–34

Contents lists available at ScienceDirect

Developmental Biology

journal homepage: www.elsevier.com/locate/developmentalbiology

Identification of the genes encoding candidate septate junction components expressed during early development of the sea urchin, *Strongylocentrotus purpuratus*, and evidence of a role for Mesh in the formation of the gut barrier

Sima Jonusaite [a,*], Nathalie Oulhen [b], Yasushi Izumi [c], Mikio Furuse [c,d], Takashi Yamamoto [e], Naoaki Sakamoto [e], Gary Wessel [b], Andreas Heyland [a]

[a] Department of Integrative Biology, University of Guelph, Guelph, ON N1G 2W1, Canada
[b] Department of Molecular and Cell Biology and Biochemistry, Brown University, Providence, RI, 02912, United States
[c] Division of Cell Structure, National Institute for Physiological Sciences, Okazaki, 444-8787, Japan
[d] Nagoya University Graduate School of Medicine, Aichi, 464-8601, Japan
[e] Division of Integrated Sciences for Life, Graduate School of Integrated Sciences for Life, Hiroshima University, Hiroshima, 739-8526, Japan

ARTICLE INFO

Keywords:
Sea urchin
Epithelial development
Septate junctions
Mesh
Intestinal barrier
CRISPR/Cas9

ABSTRACT

Septate junctions (SJs) evolved as cell-cell junctions that regulate the paracellular barrier and integrity of epithelia in invertebrates. Multiple morphological variants of SJs exist specific to different epithelia and/or phyla but the biological significance of varied SJ morphology is unclear because the knowledge of the SJ associated proteins and their functions in non-insect invertebrates remains largely unknown. Here we report cell-specific expression of nine candidate SJ genes in the early life stages of the sea urchin *Strongylocentrotus purpuratus*. By use of in situ RNA hybridization and single cell RNA-seq we found that the expression of selected genes encoding putatively SJ associated transmembrane and cytoplasmic scaffold molecules was dynamically regulated during epithelial development in the embryos and larvae with different epithelia expressing different cohorts of SJ genes. We focused a functional analysis on SpMesh, a homolog of the *Drosophila* smooth SJ component Mesh, which was highly enriched in the endodermal epithelium of the mid- and hindgut. Functional perturbation of SpMesh by both CRISPR/Cas9 mutagenesis and vivo morpholino-mediated knockdown shows that loss of SpMesh does not disrupt the formation of the gut epithelium during gastrulation. However, loss of SpMesh resulted in a severely reduced gut-paracellular barrier as quantitated by increased permeability to 3–5 kDa FITC-dextran. Together, these studies provide a first look at the molecular SJ physiology during the development of a marine organism and suggest a shared role for Mesh-homologous proteins in forming an intestinal barrier in invertebrates. Results have implications for consideration of the traits underlying species-specific sensitivity of marine larvae to climate driven ocean change.

1. Introduction

A unifying characteristic of metazoan evolution is the emergence of epithelial tissues that form a physical barrier between the environment and the coelomic cavity, and between different compartments within the body, allowing for organismal maintenance of internal osmotic and chemical milieu. To accomplish these functions, epithelial cells have evolved specialized intercellular junctions, designated as occluding junctions, that regulate free diffusion of ions, water, and other solutes across epithelial layers through the paracellular (i.e. between cells) pathway (Jonusaite et al., 2016). The permeability of the paracellular pathway in the epithelia of vertebrates is controlled by tight junctions (TJs) which form continuous strands around the most apical cell borders and seal the paracellular space between adjacent cells (Anderson and Van Itallie, 2009; Furuse, 2010). Invertebrate epithelia generally lack TJs and instead possess septate junctions (SJs) as their occluding junctions which lie in circumferential belts around the apicolateral cell membranes and have ladder-like septa spanning the intercellular space between the cells

* Corresponding author. Department of Integrative Biology, Faculty of Biological Sciences, University of Guelph, Guelph, ON N1G 2W1, Canada.
E-mail address: sjonusai@uoguelph.ca (S. Jonusaite).

https://doi.org/10.1016/j.ydbio.2022.12.007
Received 7 July 2022; Received in revised form 20 December 2022; Accepted 22 December 2022
Available online 29 December 2022

(Green and Bergquist, 1982; Jonusaite et al., 2016). Substantial differences in the fine details of SJ morphology have been revealed to exist across invertebrate phyla and some animals possess multiple types of SJs specific to different epithelia (Jonusaite et al., 2016b). As an integral component of internal and external epithelia, SJs play significant roles in the physiology of invertebrates, including those life stages that rely on aquatic habitats which can change rapidly due to environmental, climatic, and anthropogenic factors (Jonusaite et al., 2016, 2017a,b; Nowghani et al., 2019; Venn et al., 2020).

Genes encoding proteins that form SJs have been identified and tested in the model invertebrate, *Drosophila melanogaster,* which like other insects and more generally arthropods have two morphological SJ variants, the ectodermal pleated SJs (pSJs) and the endodermal smooth SJs (sSJs), respectively (Green et al., 1979; Green, 1981; Izumi and Furuse, 2014). Over thirty SJ associated proteins have been identified in *Drosophila*, including plasma membrane spanning proteins as well as cytoplasmic adaptor and signaling molecules (Izumi and Furuse, 2014; Jonusaite et al., 2016; Izumi et al., 2021; Rice et al., 2021; Rouka et al., 2021). It is now also evident that in addition to establishing and/or regulating the SJ barrier, a large number of *Drosophila* SJ proteins are required for cell- and tissue-specific morphogenetic and cellular signaling events during and post-embryogenesis (Zeng et al., 2010; Hall and Ward, 2016; Rice et al., 2021; Rouka et al., 2021; Izumi et al., 2021; Resnik-Docampo et al., 2021; Jonusaite and Rodan, 2021). The biological significance of the presence of multiple morphologically distinct epithelial SJs in other invertebrates is unclear because of a lack of molecular SJ studies in diverse animal representatives. As such, the identity and roles of SJ proteins during and after development in non-insect species remain largely unknown.

Echinoderms are a diverse and abundant group of marine invertebrates with ecological, scientific, and economic importance. Their external fertilization and development and the transparency of embryos coupled with the availability of molecular tools for gene perturbation have made echinoderms prime organisms to explore fundamental questions in development and cell biology (McClay, 2011; Arnone et al., 2015; Lin et al., 2019; Adonin et al., 2021). Two unique SJ variants have been observed in the epithelia of echinoderms, the ectodermal double-septum SJs and the endodermal anastomosing SJs, but their molecular physiology remains unknown (Green et al., 1979; Green, 1981). A large group of echinoderms live part of their life cycle as free-swimming larvae and given that the major larval epithelia, the body wall ectoderm and the gut, are in direct contact with the seawater, the contributions of SJs and their proteins to the formation and function of these epithelia are likely essential for controlled physiology during development of the animal.

The goal of the current study was to identify the diversity, expression characteristics, and function of SJ proteins in a non-insect invertebrate during development using the purple sea urchin, *Strongylocentrotus purpuratus*. We first identified *S. purpuratus* genes belonging to the families that, in *Drosophila*, include members encoding SJ components, and monitored their cell-specific expression from hatched blastula to early pluteus larva using *in-situ* hybridization and single-cell mRNA sequencing (scRNAseq) analysis. Our results revealed spatiotemporal expression of candidate SJ genes in the developing ectoderm and endodermal gut epithelia and that SpMesh, an ortholog of *Drosophila* smooth SJ component Mesh, is essential for fidelity of the gut barrier function in larval sea urchin. These data provide the first insight into the candidate components of epithelial SJs during the development of an aquatic non-insect invertebrate and evidence for the shared function of Mesh in regulating intestinal SJ barrier. The work lays the foundation for future studies to consider the roles of SJ proteins in the developmental physiology of marine invertebrates in times of global scale ocean changes.

2. Materials and methods

2.1. Animal maintenance and embryo collection

Adult *Strongylocentrotus purpuratus* were obtained from Pete Halmay of Pt. Loma Marine Invertebrate Lab (Lakeside, CA, email: peterhalmay@gmail.com) and were maintained in the Hagen Aqualab (University of Guelph, Ontario, Canada) in artificial seawater (made from Instant Ocean sea salt) on a 12:12 light cycle in recirculating artificial seawater (ASW) at 12 ^{0}C and 34 ppt salinity. Adult urchins were fed rehydrated sugar kelp (*Saccharina latissima*) ad libitum throughout the year. For *mesh* CRISPR/Cas9 approaches, adult *S. purpuratus* were housed in 35 ppt artificial seawater at 16 °C. Adult urchins were spawned via intra-coelomic injection with 1 ml of 0.5 M KCl. The eggs were collected by inverting the females over a small glass beaker filled with filtered ASW (FASW) and the sperm was collected dry with a small plastic pipette. Several drops of highly diluted sperm ($1/10^6$) were added to the eggs and fertilization success tested after 10 min by detection of the fertilization envelope. Fertilized eggs were transferred to a 1L beaker with FASW at 12 ^{0}C and different stage embryos collected over the 3 day period. For *mesh* CRISPR experiments, embryos were cultured in filtered seawater collected from Woods Hole, Massachusetts, in Corning Nunc® IVF dishes at 16 °C.

2.2. RNA extraction and cDNA synthesis

To extract total RNA, embryos were collected directly into 500 μl of TRIzol® Reagent (Ambion) in 1.5 ml microcentrifuge tubes, homogenized using a plastic pestle and RNA extracted using the Direct-zol™ RNA MiniPrep Kit (Zymo Research) as per manufacturer's instructions. All RNA samples were treated with DNAse I (Zymo Research) to remove any genomic DNA contamination. The quality and yield of RNA were determined using a NanoDrop 8000 spectrophotometer and template cDNA was synthesized using Applied Biosystems cDNA synthesis kit as per manufacturer's instructions. cDNA was stored at -20 ^{0}C.

2.3. Probe generation and whole mount in situ hybridization

RNA probes for *S. purpuratus* genes of interest were synthesized using cDNA templates amplified by RT-PCR with primers listed in Table 1 and with a T7 promoter site incorporated into either the forward (for sense probe transcription) or reverse (for antisense probe transcription) primer. Amplicon sequence identity and specificity was confirmed after sequencing at Core Genomics Facility (University of Guelph) and using the Blastn search algorithm against the Sp genome v5 database. RNA antisense and sense probes were transcribed using digoxigenin (DIG) RNA Labeling Mix with T7 RNA polymerase (Roche) according to manufacturer's instructions.

Embryos were fixed in 4% paraformaldehyde (PF) in FASW overnight at 4 ^{0}C. Embryos then were washed in 100% methanol and stored at -20 ^{0}C. On the day of hybridization, samples were washed 3x for 5 min each in 1x TBST (Tris Buffered Saline with 0.1% Tween-20) and then incubated at RT for 5 min each in 25%, 50%, and 75% hybridization buffer (HB) in 1x TBST (HB: 50% deionized formamide, 10% polyethylene glycol 8000 (Fisher Bioreagents), 0.6 M NaCl, 0.02 M Tris-HCl (pH 7.5), 0.5 mg/ml yeast tRNA, 1x Denhardt's solution, 0.1% Tween-20, 5 mM EDTA). The samples were pre-hybridized in 100% HB for 1 h at 62 ^{0}C. After that, the embryos were hybridized with 1–2 ng/μl of antisense and sense probes in HB overnight at 62^0 C. Probes were removed and embryos washed for 15 min in 1:1 ratio of HB:TBST, 3 × 15 min in TBST, 2 × 15 min in 1x SSCT (Saline-Sodium Citrate in TBST), 15 min in 0.1x SSCT at 62 ^{0}C. After these stringent washes the embryos were washed 2 × 5 min in TBST and incubated in blocking solution (10% goat serum and

Table 1
Strongylocentrotus purpuratus orthologs of *Drosophila* SJ-related proteins and primers used for RT-PCR and in situ hybridization probe synthesis.

Protein	*S. purpuratus* gene name	Primer sequence	Amplicon length, bp	GenBank accession number
Tetraspanin-2A (Izumi et al., 2016)	*Sp_tetraspanin*	For 5′-GCTCGTCGTCGCAGTAGTAT-3′ Rev 5′-GTTGCGTTGGTGGGTGTTAC-3′	818	XM_030988787
Mesh (Izumi et al., 2012)	*Sp_sushi-domain containing protein 2/mesh*	For 5′-CACAGCAGACCTTCACCGAT-3′ Rev 5′-AACGTGACTCCAACTGCGAT-3′	964	XM_030977979
Contactin (Faivre-Sarrailh et al., 2004)	*Sp_contactin 2*	For 5′-AGCAGCCAGAGGAAACCATC-3′ Rev 5′-TCCTCAGCCTCTACGTTCCA-3′	961	XM_030973491
Neuroglian (Genova and Fehon, 2003)	*Sp_neurofascin/neuroglian-like 2*	For 5′-GTTGCATCAAACACGGGAGG-3′ Rev 5′-CCGCCATCCACTTTCTTGAC-3′	572	XM_030973465
Discs large (Woods et al., 1996)	*Sp_disks large homolog 1*	For 5′-GGCAAGGTTACGGAGTGTCA-3′ Rev 5′-CTTGGCTGTGCAATGTCGTC-3′	922	XM_030982147
Lethal(2) giant larvae Strand et al. (1994)	*Sp_lethal(2) giant larvae protein homolog 2*	For 5′-TCGTTTCGGTGTCCAGAAGG-3′ Rev 5′-CACACTCGTGCTGAACCTCT-3′	926	XM_030984176
Coracle/Protein 4.1 homolog (Lamb et al., 1998)	*Sp_protein 4.1*	For 5′-GAGGATGAGCACCCAGTGTT-3′ Rev 5′-TCTAGCGACCTCTTCCTCCA-3′	456	XM_011676012
Melanotransferrin/Transferrin 2 (Tiklová et al., 2010)	*Sp_melanotrans-ferrin*	For 5′-CTTCCAAACTGTCCTCGCCC-3′ Rev 5′-CGACATCATAGCTCTCCCCG-3′	452	XM_030982726
Na^+/K^+-ATPase subunit alpha (Paul et al., 2003, 2007)	*Sp_Na^+/K^+ -ATPase alpha subunit*	For 5′-GGGTATCGCTGGGAGTGATG-3′ Rev 5′-GCTGTCGTGATAGGGGATGG-3′	1068	NM_001123510
Na^+/K^+-ATPase subunit beta 2/Nervana 2 (Paul et al., 2003, 2007)	*Sp_Na^+/K^+ -ATPase subunit beta-1*	For 5′-ATGGGCGGTGATGACGATAC-3′ Rev 5′-CGGAGAGACGTAGAGAGCCT-3′	753	XM_774822
Zonnula occludens-1 (ZO-1) Fanning and Anderson (2009)	*Sp_tight junction protein ZO-1*	For 5′-ATCAAACCAGGTAGCCCTGC-3′ Rev 5′-ATATCCTTGACCTGCGAGCG-3′	920	XM_777594

1% BSA in TBST) for 1 h at RT. Anti-DIG antibody coupled to alkaline phosphatase (Roche) was added at a dilution of 1:2000 in antibody dilution buffer (5% goat serum and 1% BSA in TBST) and embryos left overnight at 4 ^{0}C. Following this, the embryos were washed 3 × 5 min in TBST and equilibrated 2x at 5 min in an alkaline phosphate buffer (AP: 100 mM NaCl, 50 mM $MgCl_2$, 100 mM Tris-HCl (pH 9.5), 0.1% Tween 20, and 1 mM levamisole hydrochloride (MP Biomedicals)). The embryos were then incubated in NBT/BCIP (Roche) in AP + 2% dimethyl formamide for colour reaction and the staining stopped with 2 × 5 min washes in TBST + 50 mM EDTA. The embryos were mounted in 30% glycerol in TBST and imaged using Nikon Eclipse Ti2 microscope equipped with a DS-Fi3 colour camera.

2.4. Gene expression analysis using single cell RNA sequencing

Single cell RNA-seq datasets used here were previously generated by Foster et al. (2020) for *S. purpuratus* early developmental time points (8-cell, 64-cell, morula, early blastula, hatched blastula, mesenchyme blastula, early gastrula and late gastrula stages) and by Perillo et al. (2020) for early pluteus (72 hpf) stage. For the early time points, the embryos were fully dissociated and all the resulting cells were used for the scRNAseq analysis. For the late time point (72 hpf), the plutei were only gently dissociated, leading to an enrichment of the ectodermal cells used for this scRNAseq dataset. The t-SNE (t-distributed stochastic neighbor embedding) projection and clustering analysis for visualization of the integrated data was obtained using the R package Seurat v 3.1.4 with 15 parameter dimensions and resolution of 0.5.

2.5. Phylogenetic analysis

The phylogenetic analysis was conducted using Geneious software (2022.2). Each reference sequence from *Drosophila* (Table S1) was blasted again species-specific protein database for coral, sea urchin, zebrafish, mouse and human and the top 10 hits were retrieved (Supplemental file 1). For each group of proteins alignments were done using Genious Clustal Omega algorithm (Global alignment with free end gaps, Blosum62 cost matrix, open gap penalty – 12, Gap extension penalty – 2, Refinement iteration – 2) and phylogenetic analysis was conducted for that alignment using UPGMA/Jukes-Cantor genetic distance model with 100,000 bootstrap replicates using sequences from all species and the *Drosophila* reference sequence. Additionally, the 10 sea urchin sequences for each group were aligned against *Drosophila* reference sequences (Global alignment with free end gaps, Blosum62 cost matrix, open gap penalty – 12, Gap extension penalty – 2, Refinement iteration – 2) and phylogenetic analysis using UPGMA/Jukes-Cantor genetic distance model with 100,000 bootstrap replicates was conducted. In addition to

phylogeny approach, selection of target *S. purpuratus* sequences from each group for further examination was also based on previously published references for *Sp_mesh* (Izumi et al., 2012), *Sp_tetraspanin* (Love et al., 2007), and *Sp_Na$^+$/K$^+$ -ATPase alpha* (Lee et al., 2019) and manual analysis of protein domain architecture and known functional groups (https://myhits.sib.swiss/cgi-bin/motif_scan; http://gpcr.biocomp.unibo.it/predgpi/pred.htm; http://smart.embl-heidelberg.de/smart/set_mode.cgi; Ganot et al., 2015; Rouka et al., 2021).

2.6. Antibody generation and validation

To generate polyclonal anti-Mesh antibodies, the C-terminal cytoplasmic region of *Hemicentrotus pulcherrimus mesh* was amplified based on the sequence of *Strongylocentrotus purpuratus mesh* (Entrez gene symbol: LOC580458) using prism larval cDNA and the following primers: forward 5′ acgcgtcgacAAAACCAATAGCAGCTACCCAAGGAAATCG-3'; reverse 5′-acgcgtcgacCTAAATCCACCCACCAGTACCTTTGATGGT-3'. The amino acids encoding the C-terminal region of the HpMesh protein (Fig. S2) were cloned into a Sal I site of pGEX-6P-3 (GE Healthcare) to produce a Glutathione S-transferase fusion protein. The protein was expressed in *Escherichia coli* (DH5α) and purified using Glutathione Sepharose 4B (GE Healthcare). Polyclonal antibodies were generated in rabbits [7-1 and 7-2] by Kiwa Laboratory Animals (Wakayama, Japan). The specificity of the antibodies was tested in *S. purpuratus* using immunofluorescence and Western Blotting (Fig. 4) with preimmune serum as controls (performed as described below).

2.7. Fluorescence Immunolocalization

Different stage embryos were fixed in 4% PF in FASW for 15–30 min at RT and rinsed 3 × 10 min in 1x PBST (Phosphate Buffered Saline with 0.3% Tween-20). The samples were incubated for 1 h at RT in blocking solution (2% BSA and 1% goat serum in PBST) and probed with primary antibodies overnight at 4 ^{0}C. The following antibodies diluted in blocking solution were used: rabbit anti-HpMesh 7-1 and 7-2 (1:1000), and mouse anti-Na$^+$/K$^+$-ATPase alpha subunit (NKA; 1:10; a5, Developmental Studies Hybridoma Bank; Stumpp et al., 2015) As negative controls, samples were incubated with preimmune serum (at 1:1000 for Mesh) or blocking solution alone (for NKA). Following incubation, samples were washed 5 × 5 min in PBST and incubated for 3 h at RT with either FITC-conjugated goat anti-rabbit (62–6511; Invitrogen) or Alexa Fluor 488-conjugated goat anti-mouse (A-11001; Invitrogen) secondary antibodies diluted in PBST (1:400). The samples were then rinsed in PBST 3 × 5 min and incubated in 4',6-diamidino-2-phenylindole (DAPI) DNA stain (1:3000 in PBST) for 5 min. After rinsing the samples 2 × 5 min in PBST and 2 × 5 min in PBS, they were mounted in glycerol with DABCO (90% glycerol, 0.1 M Tris-HCl (pH 8.5), 10% 1,4-Diazabicyclo[2.2.2]octane (DABCO; Sigma)) and imaged using either Leica TCS SP5 laser-scanning confocal microscope or Nikon Eclipse Ti2 epifluorescence microscope with the accompanying Leica LAS AF or NIS Elements acquisition software, respectively.

2.8. Vivo-morpholino design and delivery

Vivo-Morpholinos (vMOs) are antisense oligonucleotide analogues designed to enter the cell by crossing the plasma membrane without further necessary manipulation and bind to complementary RNA sequences to block the translation of the target gene (Ferguson et al., 2014). Studies have shown that vMO treatment of sea urchin embryos and larvae result in knockdown phenotypes in skeleton development, BMP signaling and midgut ion transport (Luo and Su 2012; Heyland et al., 2014; Petersen et al., 2021). In the current study, we used a vMO (obtained from Gene Tools, US) designed against the *Spmesh* gene with the sequence 5′-AATTTCAGACAGATTCCCAAAGACG-3′ complementary to the 5′UTR region 13 nucleotides upstream of the translation start codon. For a negative control, a standard control vMO with the sequence 5′-CCTCTTACCTCAGTTACAATTTATA-3′ was employed similarly.

For initial vMO treatments, late gastrula stage embryos (~48 hpf, when Mesh mRNA transcripts are first detected by scRNA seq, Fig. 3) were collected in 1.5 ml microtubes and exposed to 500 μl FASW containing 1 μM, 2.5 μM and 5 μM *Spmesh* or control vMO, or milliQ water (as a carrier control used to dilute vMO stock solutions). The embryos were incubated for 24 h at 14 ^{0}C to allow them to reach the early pluteus stage (72 hpf) as this is the oldest stage used in all of the experiments. We chose 2.5 μM vMO concentration as the final working concentration since exposure to 5 μM *Spmesh* or control vMO reduced larval swimming activity (the larvae looked normal otherwise; data not shown), suggesting a non-specific effect of this concentration of vMOs on early larvae. Following 2.5 μM vMO treatments, the larvae were collected for FITC-dextran permeability assay and quantification of Mesh protein abundance (performed as described below).

2.9. Synthetic guide RNA (gRNA) design, microinjection and CRISPR induced genomic mutation analysis

Synthetic gRNAs were designed against the 4th exon of *Spmesh* gene using CRISPRscan software (https://www.crisprscan.org/) and only those with no predicted off-target binding sites in the genome were selected for use in this study (Table 2). The Cas9 protein (IDT 1081059, 2 μM final concentration) was mixed with each individual gRNA (31 μM final concentration) and incubated at RT for 5 min to enable their binding before starting the injections. 10,000 MW dextran conjugated with Texas red (Thermo Fisher) was then added to a final concentration of 1.25 mM for detection of injected embryos. Microinjection of *S. purpuratus* eggs was performed as described previously (Oulhen and Wessel, 2016). Briefly, the eggs were de-jellied with acidic seawater (pH 5.0) for 10 min and washed 3 x with FASW. The eggs were then rowed onto protamine sulfate-coated 60 × 15 mm Petri dishes (Fisher Scientific 12-566-353), fertilized in the presence of 1 mM 3-Amino-1,2,4-triazole (Sigma A8056) and over 100 embryos were injected in each of three separate biological experiments using the Femto Jet® injection system (Eppendorf; Hamburg, Germany).

Assessment of genomic mutations generated by CRISPR/Cas9 was accomplished by sequence trace decomposition analysis using TIDE (Tracking of Indels by Decomposition; https://tide.nki.nl/), a freely available bioinformatics tool. The genomic DNA of individual larva from either the control injections (Cas9 only) or the *mesh* knock-out injections (Cas9+gRNA) was extracted with 12 μl of QuickExtract DNA Extraction Solution (Lucigen) according to manufacturer's instructions. 2.5 μl of this extraction mix was then subjected to PCR amplification of *Spmesh* genomic DNA region encompassing gRNA target sites. At least 10 individual larvae were used for each condition. The PCR products from single larva were isolated using standard column DNA purification reagents and were Sanger sequenced with either the forward or the reverse primers used to generate the PCR products. The resulting sequencing data (.ab1) were subjected to TIDE by direct sequence analysis for overall mutation efficiency and indel (insertion + deletion) frequencies at the gRNA target site (Brinkman et al., 2014). Based on TIDE estimates, the highest efficiency of CRISPR-induced mutagenesis was achieved using *Spmesh* gRNA 346 (Fig. S3) which was subsequently used in FITC-dextran permeability assay (described below). The primers used for PCR amplification of genomic DNA region with gRNA 346 induced mutations were: forward 5′-GACAAATACATACACAAAATATACCG-3′, reverse 5′-GTAAATAGA TTAAATAAACATGAGTTGATAC-3'.

Table 2
CRISPR gRNA sequences.

Sequence name	gRNA sequence
Sp_mesh 306	5′-CGACGGGCGAATTGAGGACC-3′
Sp_mesh 346	5′-GGGGCCGATGTAGATATTAC-3′
Sp_mesh 450	5′-GGCTAAAGTCGACATTGCTC-3′

2.10. Western blotting

72 h pluteus larvae were mixed with 3-fold volume of RIPA lysis buffer (50 mM Tris-HCl, pH 7.8, 150 mM NaCl, 0.1% sodium deoxycholate, 1% Triton-X-100, 0.1% SDS, 1 mM EDTA), homogenized using a plastic pestle in 1.5 ml microcentrifuge tubes, centrifuged at 13,000*g* for 10 min at 4 ^{0}C, and protein content of the collected supernatants determined using a Bradford assay (Sigma-Aldrich) with a bovine serum albumin standard curve. Samples (10–15 μg protein) were prepared for SDS-PAGE by heating for 5 min at 95 °C in a 4x SDS loading buffer (200 mM Tris-HCl (pH 6.8), 8% (w/v) SDS, 40% (w/v) glycerol, 50 mM EDTA, 0.08% (w/v) bromophenol blue, and 588 mM β-mercaptoethanol). Proteins were electrophoretically separated on 10% SDS denaturing polyacrylamide gels and transferred to PVDF membranes (Millipore) using a tank blotting system (Bio-Rad). The membranes were blocked with 5% powdered fat-free milk in TBS-T for 1 h at RT, and probed overnight at 4 ^{0}C with anti-Mesh primary antibodies (7-1, 7-2) or preimmune serum diluted at 1:1000. After washing with TBST, membranes were incubated for 1 h with horseradish peroxidase (HRP)-conjugated goat anti-rabbit IgG secondary antibody (32460; Invitrogen) diluted at 1:5000 and antigen reactivity visualized using Clarity™ Western ECL substrate (Bio-Rad) and a Chemidoc Imaging system. For visualization of actin, the membranes were stripped with stripping buffer (20 mM magnesium acetate, 20 mM KCl, 0.1 mM glycine, pH 2.2) for 30 min and re-probed with 1:5000 dilution of mouse monoclonal anti-β-actin antibody (A5441; Sigma), followed by HRP-conjugated goat anti-mouse IgG secondary antibody at 1:5000 (31430; Invitrogen). Densitometric analysis of Mesh and actin was conducted using Image J and Mesh expression was reported as a normalized value relative to the abundance of actin.

2.11. FITC-dextran permeability assay

Fluorescently labeled dextran has been previously used to assess epithelial paracellular permeability in larval green sea urchin and other invertebrates (Stumpp et al., 2012; McMillan et al. 2017; Kolosov et al., 2019; Jonusaite et al., 2020). To examine the effects of vMO knockdown and CRISPR mutation of *mesh* on dextran permeability in *S. purpuratus* early pluteus larvae (~72 hpf), collected animals were concentrated in 1.5 ml microtubes by brief centrifugation and FASW replaced with fresh FASW containing 0.5 mg/ml fluorescein isothiocyanate-labeled dextran (FITC-dextran, 3–5 kDa; Sigma). The larvae were incubated in FASW with FITC-dextran for 15 min at 14 ^{0}C. Depletion of divalent cations is known to disrupt epithelial paracellular barrier in sea urchin embryos and can serve as a positive control of increased SJ permeability (Itza and Mozingo, 2005). For the positive control group in our studies, a set of larvae were briefly immersed in Ca^{2+}/Mg^{2+}-free SW (461 mM NaCl, 10.7 mM KCl, 2.14 mM $NaHCO_3$) prior to adding FASW with FITC-dextran. Following FITC-dextran incubation, all larvae were washed 3 x in FASW and loaded into 35 × 35 mm CELLview™ glass bottom dish (627871; Greiner Bio-One, Germany) that had been pre-coated with poly-L-lysine to immobilize larvae for imaging. For *mesh* vMO knockdown study, the larvae were imaged under 20x objective lens using inverted Nikon Eclipse Ti2 epifluorescence microscope with a 488 nm excitation and 555 nm emission filter, with 0 gain and 30 ms exposure time. Using these settings, a z-stack of 20-25 optical sections of 3 μm increments were captured across each larva and another z-stack of images taken in an area with no animals for background fluorescence correction. For the *mesh* CRISPR study (performed at Brown University), the larvae were imaged using a Nikon Yokogawa W1 spinning disk confocal microscope. Analysis of all images was completed in ImageJ. The fluorescence intensity inside the larvae was measured as the sum of raw integrated densities (RIDs) of each section within the z-stack of selected area after background fluorescence RID subtraction.

2.12. Statistical analysis

Data for FITC-dextran permeability assay and protein abundance were analyzed using GraphPad Prism (version 9) and are reported as means ± SE (N). Comparisons between groups were conducted using one-way ANOVA followed by Tukey's multiple comparisons of the mean with a significance level of $P < 0.05$. FITC-dextran assay data from *mesh* CRISPR experiment were not normally distributed and were analyzed by Kruskal-Wallis one-way ANOVA and post-hoc Dunn's multiple comparisons test. Gene expression from the single cell RNA seq datasets were analyzed using the R package Seurat.

3. Results

3.1. Developing epithelia of the sea urchin express distinct cohorts of candidate septate junction genes

The existence of morphologically different SJs in the epithelia of echinoderms and other invertebrates raises the question of whether the morphological differences reflect the differences in the molecular architecture and functions of various SJs. To begin the molecular characterization of echinoderm SJs, we used the NCBI database to search *S. purpuratus* genome for *Drosophila* pSJ- and sSJ-associated protein orthologs. The search was performed in an iterative manner, first targeting *S. purpuratus* and then extended to include representative species of a non-bilaterian (coral) and vertebrates with up to 10 most closely related sequences selected for each protein group and subjected to phylogenetic analyses (Fig. S1; Supplemental file 1). We used phylogenetic trees (Fig. S1), protein domain composition analysis, and previously published references, when available, to select target *S. purpuratus* sequences from each protein group for further studies. Our examination of the selected candidate *S. purpuratus* SJ genes by in situ hybridization and scRNAseq analysis revealed that their expression was highly variable in the developing epithelia of the embryos and larva (Figs. 1 to 3 and Fig. S4). Expressions of these genes in the scRNAseq datasets are represented as feature plots and are described in detail in the legends of Figs. 2 and 3.

3.1.1. Early embryonic ectoderm enriched putative SJ genes

The candidate SJ genes whose mRNA transcripts were detected by both in situ hybridization and scRNAseq from the earliest tested hatched blastula stage were *Sp_tetraspanin (tspn)*, *Sp_tight junction protein ZO-1 (ZO-1)* and *Sp_melanotransferrin (mtf)* (Figs. 1 and 2; Table 1). In the blastula (20 hpf) and early gastrula (28 hpf) stages, the expression of both *Sptspn* and *SpZO-1* was enriched specifically in the animal pole ectoderm whereas *Spmtf* was distributed more broadly throughout the ectodermal cells (Fig. 1). In the later stages, *Sptspn* retained the ectodermal expression and was enriched in the apical and aboral ectoderm in the prism and pluteus larvae (Figs. 1 and 2A), while *SpZO-1* showed increased expression in the endodermal gut cells (Figs. 1 and 2B). *Spmtf* expression in the ectodermal cells declined progressively and shifted to the gut endoderm post-gastrulation (Figs. 1 and 2C). We further observed an early broad ectodermal expression of *Sp_contactin* (*cont*) but its mRNA transcripts in the blastula and early gastrula stages were detected by scRNAseq only. At later stages, *Spcont* expression was also seen in the endodermal gut cells (Figs. 1 and 2D).

We also analyzed the expression of *S. purpuratus* orthologs of the P-type ion transporter Na^+/K^+-ATPase (NKA) alpha and beta subunits which are required for SJ formation and morphogenesis of several epithelia in *Drosophila* and some evidence suggest ion transport-dependent and -independent roles of NKA in the organization and permeability of vertebrate TJs (Paul et al., 2003, 2007; Laprise et al. 2009; Rajasekaran et al., 2001, 2007; Krupinski and Beitel, 2009; Vagin et al., 2012). We hypothesized that NKA might be associated with SJs in

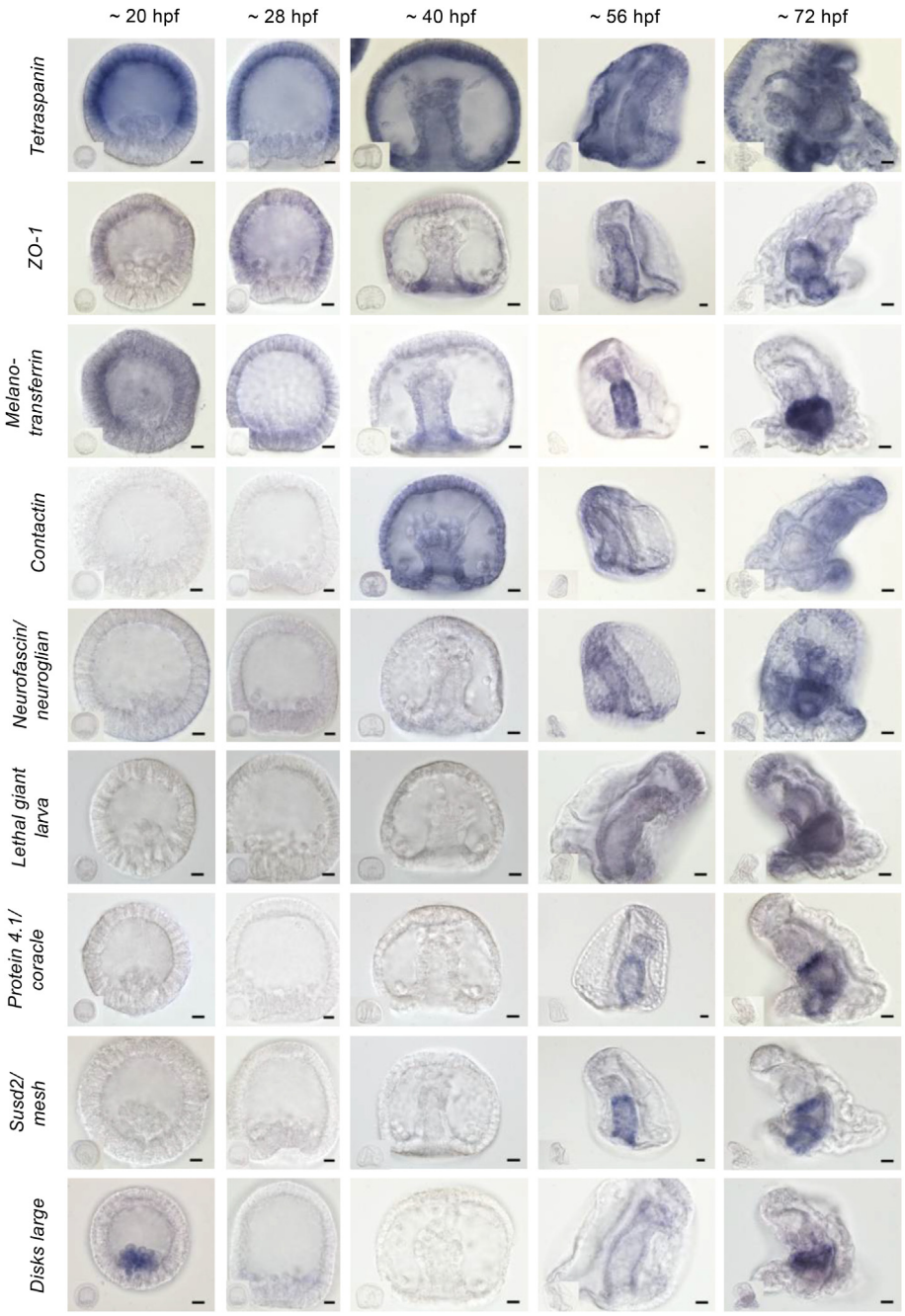

Fig. 1. Septate junction gene orthologs show temporal and spatial expression in the developing epithelia of *Strongylocentrotus purpuratus*. Distribution of putative SJ gene transcripts were visualized by whole mount in situ hybridization. Transcripts encoding for *Sp_tetraspanin (tspn)*, *Sp_ZO-1* and *Sp_melanotransferrin (mtf)* were detected in all stages tested, i.e. mesenchymal blastula (~20 hpf), early gastrula (~28 hpf), mid/late gastrula (~40 hpf), prism larva (~56 hpf) and early pluteus larva (~72 hpf). In the blastula and early gastrula stages, *Sptspn* and *SpZO-1* expression was restricted to the animal pole ectoderm whereas *Spmtf* was distributed more broadly throughout the ectodermal cells. In the later stages, *Sptspn* retained high ectodermal expression and *SpZO-1* and *Spmtf* showed increasing abundance in the developing endodermal gut epithelium and enrichment in the midgut by 72 hpf. Except for mRNA encoding for *Sp_contactin* (*cont*), which was expressed during gastrulation, transcripts encoding for *Sp_neurofascin/neuroglian* (*nfasc/nrg*), *Sp_lethal giant larva* (*lgl*), *Sp_protein 4.1*, and *Sp_susd2/mesh* were not detected until the prism stage. In the prism and pluteus larva, *Spcont*, *Spnfasc/nrg*, and *Splgl* expression was seen in the gut, apical plate and oral ectoderm, whereas *Sp_protein 4.1* and *Spmesh* appeared to be expressed exclusively in the midgut and hindgut segments of the gut. Unlike all other SJ genes, the expression of gene encoding for *Sp_disks large homolog* (*dlg*) was detected in the PMCs of ~20 hpf blastula but disappeared by ~ 28 hpf and was later detected in the gut of prism and pluteus larvae. Inserts show sense probe negative controls. Scale bars, 10 μm. Detailed diagram of labeled tissues and cells is shown in Fig. S4.

the developing sea urchin epithelia. We found that the mRNA of both *SpNKA* α and β were highly and broadly expressed in the mesenchymal blastula and during gastrulation but declined progressively in the ectoderm and shifted to the endodermal gut and skeletogenic primary mesenchyme cells (PMCs) in prism and early pluteus stages (Fig. S6A). Further immunohistochemical analysis of NKA α revealed its localization to the apical membranes of the epithelial cells (Fig. S6B), suggesting an ion-transport associated role for NKA in these developing epithelia as previously reported for *S. purpuratus* pluteus midgut (Stumpp et al., 2015; Lee et al., 2019).

3.1.2. *Larval gut epithelia are enriched in SJ gene orthologs*

In situ hybridization analysis revealed that a set of candidate SJ genes was not expressed until late gastrulation and showed enrichment in the developing gut epithelia. These genes were *Sp_neurofascin/neuroglian* (*nfasc/nrg*), *Sp_lethal(2) giant larva* (*lgl*), *Sp_protein 4.1* (a homolog of *Drosophila* coracle), and *Sp_sushi-domain containing protein 2(susd2)/mesh* (a homolog of *Drosophila* Mesh) (Fig. 1; Table 1). In the prism and pluteus larva, in addition to the gut, *Spnrg*, and *Splgl* expression was also seen in the apical plate and surrounding ectoderm, but *Sp_protein 4.1* and *Spmesh* appeared to be expressed exclusively in the midgut and hindgut segments of the gut (Fig. 1). Albeit detected at lower levels, another larval gut associated SJ gene was *Sp_disks large homolog 1* (*dlg*) but unlike all other genes, *Spdlg* showed a transient expression in the primary mesenchymal cells (PMCs) of mesenchyme blastula (Fig. 1).

Endodermal gut cell expression of *Splgl*, *Sp_protein 4.1*, and *Spmesh* in late gastrula and larval stages was also supported by the scRNAseq (Fig. 3A–C). Of note, due to the difficulty in dissociating hindgut cells post-gastrulation, only midgut cell clusters have been detected in the analysis of 72 hpf time point (Perillo et al., 2020). Additional *Splgl* expression in the cells of the apical plate and apical ectoderm (Fig. 3A) and that of *Spdlg* in the blastula PMCs (Fig. 3D) were also detected by the

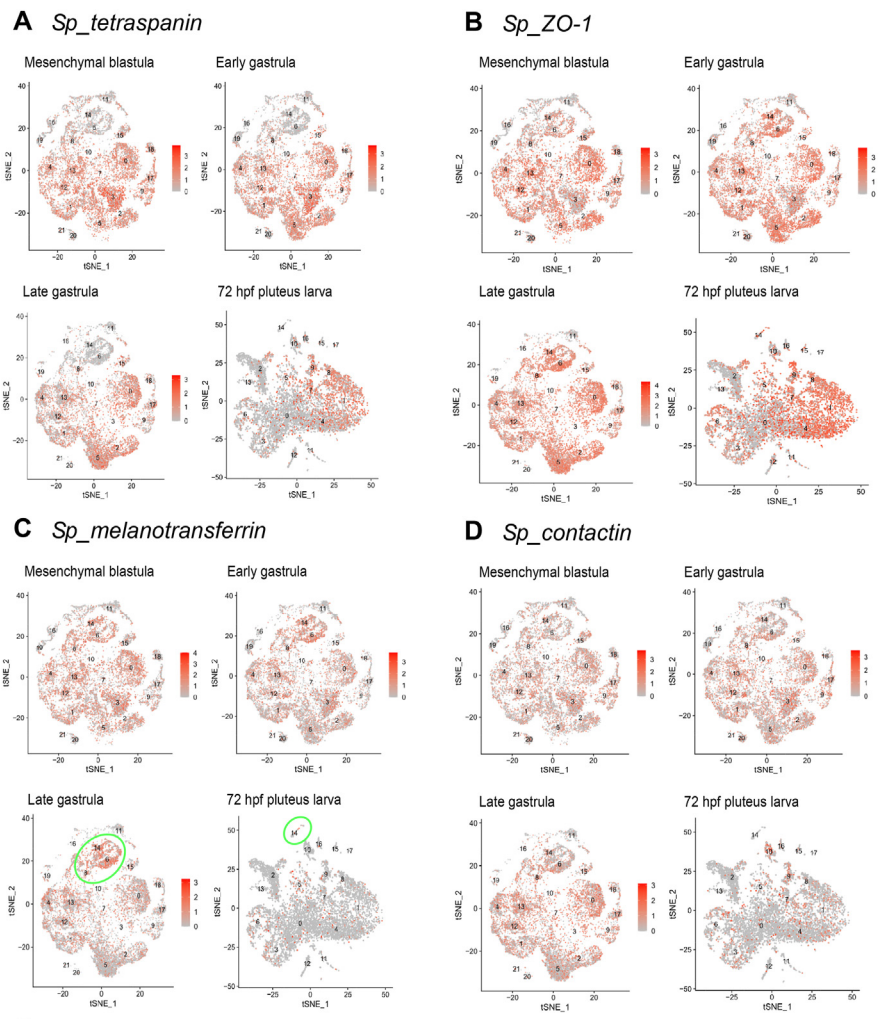

Fig. 2. Temporal and spatial expression of *Sptspn*, *SpZO-1*, *Spmtf* and *Spcont* revealed by single cell RNAseq. Feature plots colored for selected genes from datasets of Foster et al. (2020) and Perillo et al. (2020) encompassing mesenchymal blastula, early gastrula, late gastrula, and 72 hpf stages during *S. purpuratus* development. (A) *Sptspn* showed high and broad expression throughout the ectoderm in the blastula and early gastrula stages, and was enriched in the apical and aboral ectoderm cells in late gastrula and 72 hpf pluteus. (B) *SpZO-1* was expressed broadly in the ectodermal and endodermal cells across all stages. (C) In the blastula and early gastrula stages, *Spmtf* was expressed broadly throughout the ectodermal and endodermal cells but declined progressively in the ectoderm and shifted to the gut in late gastrula and pluteus stages (clusters 6, 8, and 14, circled in green). (D) *Spcont* was detected in the ectodermal and endodermal cells across all stages with lower levels at 72 hpf. Cells are colored by relative expression level in all plots. (E)The table summarizes the main cell-types with numbers and colours representing clusters in the tSNE plots.

E

Cell-clusters for MB, EG, and LG from Foster et al. 2020	
0, 5	Aboral ectoderm
1, 4, 12, 13	Oral ectoderm
2, 7	Cilliated cells
3	?
6, 8, 14	Endoderm (gut)
9, 17	Neural
11	Pigment cells
15	SMCs (gut subcluster)
16, 19	PMCs (skeleton)
20	Germline

Cell-clusters for 72 hpf pluteus larva from Perillo et al. 2020			
0	Ectoderm/uncharacterized	10	Apical plate, proneural (2)
1	Apical ectoderm	11	Skeleton
2	Differentiated pigment cells	12	Mesodermal cells
3	Ciliary band neurons (1)	13	Mitotic pigment cells
4	Apical plate/uncharacterized	14	Midgut
5	Oral ectoderm/mouth	15	Serotoninergic neurons (apical plate) (1)
6	Lateral ectoderm (right)	16	Ciliary band neurons (3)
7	Ciliary band neurons (2)	17	Serotoninergic neurons (apical plate) (2)
8	Aboral ectoderm (1)		
9	Aboral ectoderm (2)		

single cell mRNA analysis. However, undetected by in situ hybridization but revealed by scRNAseq was the enrichment of *Sp_protein 4.1* in the immune function having pigment cells in the early pluteus larva (Figs. 3B and 1).

3.2. Sea urchin mesh is a component of midgut and hindgut epithelial SJs

Having discovered that *Spmesh* is expressed exclusively in the developing larval gut, we next analyzed its protein expression pattern and subcellular localization using anti-Mesh antibodies generated against a highly conserved C-terminal region of HpMesh (Fig. S2). SpMesh encodes a single-pass transmembrane protein with the extracellular NIDO, AMOP, vWD and Sushi domains found in cell-cell and cell-matrix adhesion molecules and is an ortholog of *Drosophila* sSJ component Mesh (Figs. S1 and S5; Izumi et al., 2012; Sheets et al., 2020). Our immunohistochemical analysis revealed that consistent with the mRNA transcript expression, Mesh protein was not detected until the end of gastrulation and in prism larvae its expression was restricted to the future midgut and hindgut cells (Fig. S7 and Fig. 4A–F). Within these epithelia, Mesh was distributed along the lateral cell membranes and in the cytoplasm as well as large apical aggregates (Fig. 4A arrowheads), which might suggest that it is incorporated into the SJs during this stage. By early pluteus larva stage (~72 hpf), Mesh immunoreactivity was observed exclusively along the apico-lateral cell-cell contact regions between the cells of the midgut and hindgut where presumptive SJs reside (Fig. 4G–N). Western blot analysis revealed that Mesh was detected by both antibodies as a protein of relative molecular size of ~120 kDa in early pluteus larva (Fig. 4O) which is in close agreement with the predicted protein size of 140 kDa. Out of the two types of echinoderm SJs, the single-septum anastomosing SJ variant is found specifically in the endodermally-derived gut epithelium (Spiegel and Howard, 1983; Jonusaite et al., 2016) and our data suggest that Mesh is an echinoderm anastomosing SJ-specific component.

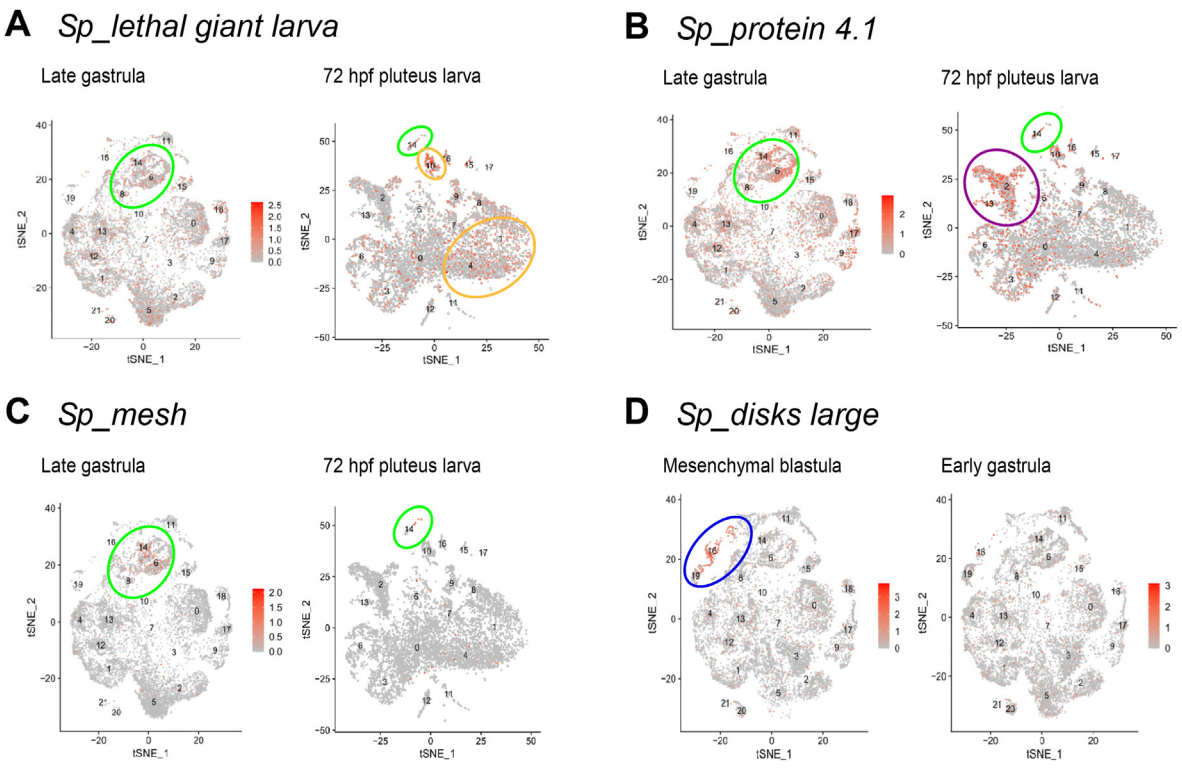

E

Cell-clusters for MB, EG, and LG from Foster et al. 2020	
0, 5	Aboral ectoderm
1, 4, 12, 13	Oral ectoderm
2, 7	Cilliated cells
3	?
6, 8, 14	Endoderm (gut)
9, 17	Neural
11	Pigment cells
15	SMCs (gut subcluster)
16, 19	PMCs (skeleton)
20	Germline

Cell-clusters for 72 hpf pluteus larva from Perillo et al. 2020			
0	Ectoderm/uncharacterized	10	Apical plate, proneural (2)
1	Apical ectoderm	11	Skeleton
2	Differentiated pigment cells	12	Mesodermal cells
3	Ciliary band neurons (1)	13	Mitotic pigment cells
4	Apical plate/uncharacterized	14	Midgut
5	Oral ectoderm/mouth	15	Serotoninergic neurons (apical plate) (1)
6	Lateral ectoderm (right)	16	Ciliary band neurons (3)
7	Ciliary band neurons (2)	17	Serotoninergic neurons (apical plate) (2)
8	Aboral ectoderm (1)		
9	Aboral ectoderm (2)		

Fig. 3. Temporal and spatial expression of *Splgl*, *Sp_protein 4.1*, *Spmesh* and *Spdlg* revealed by single cell RNAseq. Feature plots colored for selected genes from datasets of Foster et al. (2020) and Perillo et al. (2020) encompassing mesenchymal blastula, early gastrula, late gastrula, and 72 hpf stages during *S. purpuratus* development. (A) *Splgl* transcripts appeared to be enriched in the endodermal cells in late gastrula (clusters 6, 8 and 14, circled in green) as well as the midgut and the apical plate and apical ectoderm at 72 hpf (cluster 14 and clusters 1, 4 and 10, circled in green and orange, respectively). (B) *Sp_protein 4.1* showed increased expression in the endodermal cells in late gastrula (clusters 6, 8, and 14, circled green) and the pigment cells at 72 hpf (clusters 2 and 13, circled purple). (C) *Spmesh* expression was detected only in the late gastrula gut endoderm (clusters 6, 8 and 14, circled in green) and in the midgut cells of 72 hpf pluteus larva (cluster 14). (D) Expression of *Spdlg* was transiently enriched in the PMCs of the blastula stage (clusters 16 and 19, circled blue). Cells are colored by relative expression level in all plots. (E) The table summarizes the main cell-types with numbers and colours representing clusters in the tSNE plots.

3.3. CRISPR loss-of-function mesh mutant larvae have reduced gut barrier which is recapitulated by vMO mediated mesh knockdown

To gain insight into the functional role of Mesh in the developing larval gut, we targeted *Spmesh* with CRISPR/Cas9. Using *in silico* prediction tools, we designed three gRNAs targeting *Spmesh* exon 4 with no predicted off-target binding sites (Table 2). To estimate the Cas9-mediated cutting efficiency with different gRNAs, we used a Sanger sequencing based computational tool, termed Tracking of Indels by Decomposition (TIDE), which determines the spectrum and frequency of indels (insertions + deletions) generated in CRISPR/Cas9 treated sample reads near the gRNA target site relative to the wild type sequence reads (Brinkman et al., 2014). Our TIDE analysis indicated that 100% of the embryos were mutated by *Sp_346 mesh* gRNA (Fig. S3), whereas only about 40% and less than 25% of embryos were mutated when injecting with the *Sp_306* and *Sp_450 mesh* gRNAs, respectively. Based on these results, we used *Sp_346* mutants for subsequent examination.

Mesh mutant embryos developed normally up to at least early pluteus larva, which was the oldest stage tested in our study (data not shown). No apparent abnormalities were seen in the developing guts of *mesh* mutant larvae but further ongoing subcellular morphological and physiological investigations will help clarify that. In larval *Drosophila*, *mesh* knockdown causes breakdown in the barrier function of the midgut epithelium with no apparent gross morphological defects (Izumi et al., 2012). We therefore hypothesized that *mesh* mutant *S. purpuratus* larvae may have increased paracellular leak across the midgut and hindgut epithelia. To test this hypothesis, we quantified the appearance of cell-impermeable 3–5 kDa FITC-dextran in control and *mesh* mutant larvae after 15 min incubation in FITC-dextran containing SW. Depletion of divalent cations by brief exposure to Ca^{2+}/Mg^{2+}-free SW is known to disrupt epithelial SJs in sea urchin embryos (Itza and Mozingo, 2005) and we used this treatment on wild-type larvae as a positive control of increased

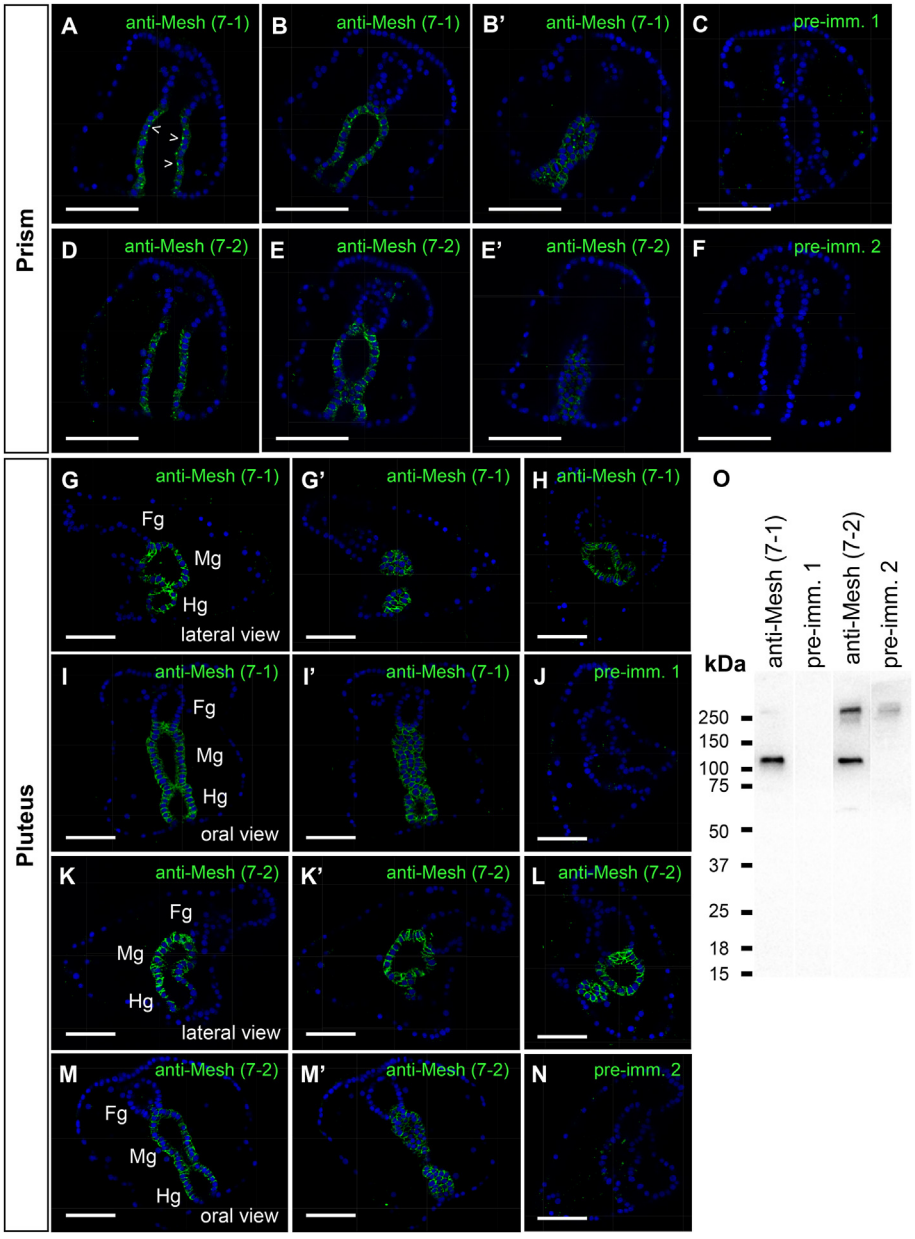

Fig. 4. Mesh localizes to SJs between the cells of the midgut and hindgut in *S. purpuratus* larvae where it is detected as ~120 kDa protein. (A-B′) Prism stage larvae stained with antibody 7-1 revealed Mesh expression in the middle and lower portions of the developing gut epithelium where it was distributed to the cell-cell contact regions between the cells as well as diffusely in the cytoplasm and as apical aggregates (arrowheads in A). B′ shows different plane optical section from larva in B. (C) No immunoreactivity was detected in prism larva incubated with preimmune serum 1. (D-E′) Prism stage larvae stained with antibody 7-2 showing Mesh immunoreactivity at the cell-cell contact regions and some in the cytoplasm of the cells of middle and lower gut segments. E′ shows different plane optical section from larva in E. (F) No immunoreactivity is detected in prism larva incubated with preimmune serum 2. (G-I′) By 72 hpf pluteus stage, Mesh is localized exclusively to the cell-cell contact regions where presumptive SJs reside between the cells of the midgut and hindgut as revealed by antibody 7-1 staining. G′ and I′ are different plane optical sections from larva in G and I, respectively. (J) No immunoreactivity was detected in pluteus larva incubated with preimmune serum 1. (K-M′) Pluteus stage larvae stained with antibody 7-2 also showed Mesh expression specifically at SJs between the cells of the midgut and hindgut. K′ and M′ are different plane optical sections from larva in K and M, respectively. (N) No immunoreactivity was detected in pluteus larva incubated with preimmune serum 2. (O) Both antibodies detected Mesh in pluteus larva as ~ 120 kDa protein which was absent in the samples incubated with preimmune serum. Nuclei counterstained with DAPI are shown in blue. Scale bars, 50 μm. Fg, foregut; Mg, midgut; Hg, hindgut.

paracellular leak across both the gut and body wall epithelia. We found that compared to control groups, *mesh* mutant larvae exhibited ~5.35 fold increase in FITC-dextran fluorescence but it was ~2.5 fold lower relative to the Ca^{2+}/Mg^{2+}-free SW treated animals (Fig. 5A–E). This disparity in leak between the Ca^{2+}/Mg^{2+}-free SW treated animals and Cas9 inactivation was predicted since the cation-depletion affects all epithelial SJs whereas the Cas9 is targeting only the gut-restricted SJ complex.

A second test of Mesh function was designed using an *Spmesh*-specific ATG-blocking vivo-morpholino antisense oligonucleotide (vMO) to knockdown *mesh* expression at the translational level. Early pluteus larvae incubated with *mesh* vMO from late gastrula/early prism stage, when *mesh* transcripts are first detected (Figs. 1 and 3), showed a significant ~50–60% reduction in ~120 kDa Mesh protein abundance compared to control and control vMO treated larvae (Fig. S8). Consistent with increased accumulation of FITC-dextran in Cas9-mediated *mesh* mutants, *mesh* knockdown larvae exhibited ~2 fold increase in FITC-dextran fluorescence compared to the control groups but it was ~7 fold lower relative to the Ca^{2+}/Mg^{2+}-free SW treated animals (Fig. 5F–J). Together, these observations suggest that Mesh is required for the intestinal barrier formation in a sea urchin larva.

4. Discussion

4.1. Epithelial specific SJ proteins function during embryonic sea urchin development

Work conducted using a model invertebrate *Drosophila* has greatly expanded our knowledge of the molecular SJ complex where over 30 proteins have been identified and shown to be required for the establishment, maturation and/or maintenance of epithelial SJs and their paracellular barrier function during embryogenesis (Rice et al., 2021; Rouka et al., 2021; Izumi et al., 2021). Along the way, it has become evident that SJ proteins are also essential for a number of developmental and cellular processes throughout the fly's life, including head involution and dorsal closure, polarization and cell shape changes and rearrangements during epithelial morphogenesis and wound closure, oogenesis and gut immune response (for detailed reviews, refer to Rice et al. (2021)

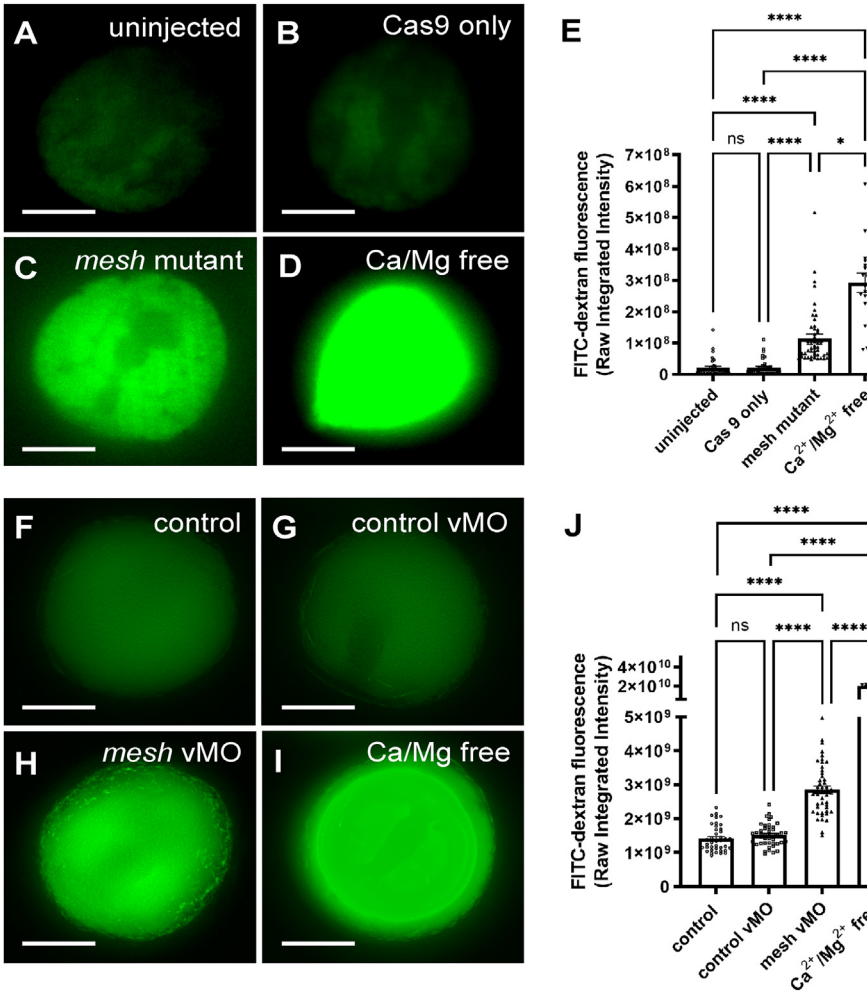

Fig. 5. CRISPR/Cas9-mediated mutation and vMO knockdown of *Spmesh* disrupt gut epithelial barrier to FITC-dextran in the early pluteus larvae. (A–D) Representative Z-stack confocal images of FITC-dextran accumulation inside uninjected control, Cas9 only control, *mesh* mutant, and Ca^{2+}/Mg^{2+}-free SW pretreated control early pluteus (72 hpf) larvae after 15 min incubation in 3–5 kDa FITC-dextran. (E) FITC-dextran fluorescence intensity was significantly greater in *mesh* mutant larvae ($1.15 \times 10^8 \pm 1.2 \times 10^7$) compared to control groups ($2.12 \times 10^7 \pm 5.1 \times 10^6$ and $2.17 \times 10^7 \pm 4.3 \times 10^6$ for uninjected and Cas9 only, respectively) but was lower relative to Ca^{2+}/Mg^{2+}-free group ($2.92 \times 10^8 \pm 3.0 \times 10^7$) which served as a positive control of increased SJ permeability in both the gut and body wall epithelia. Differences between groups were compared by one-way ANOVA (Kruskal-Wallis and *post-hoc* Dunn's tests). N = 17–49 from 3 independent experiments. $^*P < 0.05$, $^{****}P < 0.0001$. Data are expressed as means ± SE. (F–I) Representative Z-stack widefield fluorescence images of 3–5 kDa FITC-dextran accumulation inside control, vMO control, *mesh* vMO, and Ca^{2+}/Mg^{2+}-free SW pretreated control early pluteus (72 hpf) larvae after 15 min incubation in 3–5 kDa FITC-dextran containing SW. (J) FITC-dextran fluorescence intensity was significantly greater in *mesh* knockdown larvae ($2.85 \times 10^9 \pm 1.0 \times 10^8$) compared to control groups ($1.41 \times 10^9 \pm 6.0 \times 10^7$ and $1.51 \times 10^9 \pm 4.8 \times 10^7$ for control and control vMO, respectively) but was lower relative to Ca^{2+}/Mg^{2+}-free group ($2.01 \times 10^{10} \pm 1.3 \times 10^9$). Differences between groups were compared by one-way ANOVA (*post-hoc* Tukey's test). N = 40–47 from 4 independent experiments. $^{***}P < 0.0001$; ns, not significant. Data are expressed as means ± SE. Scale bars, 50 μm. For better visualization of larva in D, refer to Fig. S9.

and Rouka et al. (2021)). Unlike *Drosophila*, a large proportion of invertebrates develop and grow in aquatic habitats which can vary greatly due to a variety of abiotic and biotic stressors and it is very likely that a great deal will be learned about SJs and their proteins by uncovering their composite and functions during the ontogenesis of aquatic species. External echinoderm development in conjunction with genetic tools and functional assays offer a system to study developmental SJ physiology in a marine environment and in the epithelia that directly interface with the surrounding seawater. The importance of SJ maintained paracellular diffusion barrier has been already demonstrated in the body wall of sea urchin and starfish embryos (Itza and Mozingo, 2005; Dan-Sohkawa et al., 1995). Here we report the identification of orthologous SJ genes in the purple sea urchin and reveal functional, spatiotemporal regulation of their expression during early development.

From the free-swimming hatched blastula on, the expression of candidate *S. purpuratus* SJ genes was seen primarily in the developing ectoderm and the endodermal gut cells. Amongst the ectoderm enriched genes during gastrulation were transmembrane proteins encoding *Sp_tetraspanin* (*tspn*), *Sp_melanotransferrin* (*mtf*) and *Sp_contactin* (*cont*), and a cytoplasmic scaffold molecule coding *SpZO-1* (Figs. 1 and 2). Tetraspanins are a large superfamily of four membrane-spanning domains containing proteins with diverse roles in cell adhesion, migration, cellular activation and signalling, and *Drosophila* sSJ component tetraspanin 2A plays essential roles in the ectodermal renal epithelial development and maintenance of intestinal barrier, stem cell proliferation and differentiation (Charrin et al., 2014; Izumi et al., 2016, 2019; Beyenbach et al., 2020; Xu et al., 2019). Our observation of embryonic ectodermal enrichment of *Sptspn* is in agreement with a previous report for its orthologous gene expression in the ectoderm of two other species of sea urchin embryos (Love et al., 2007). SpMTf belongs to an iron-binding transferrin superfamily and its *Drosophila* homolog, melanotransferrin (MTf) or transferrin 2, requires iron-binding activity to mediate SJ assembly during epithelial maturation (Tiklová et al., 2010). Contactin is a GPI-linked cell-adhesion molecule and a core *Drosophila* pSJ component required for SJ organization and paracellular barrier function in the ectodermally-derived epithelia, including the salivary glands where its activity is also necessary for the lengthening of the glands during development (Faivre-Sarrailh et al., 2004; Hall and Ward, 2016). Of note, unlike *Drosophila* embryonic endoderm which lacks both Cont and MTf, we find that in *S. purpuratus* gastrula and prism larva stages, *cont* and *mtf* are also expressed in the endodermal gut cells where *mtf* becomes enriched by 72 hpf (Figs. 1 and 2 C, D), suggesting developmental roles for these proteins in both types of epithelia in a sea urchin embryo. Lastly, *Sp_ZO-1* encodes for a homolog of vertebrate TJ zonula occludens (ZO)-1 protein, a member of the membrane-associated guanylate kinase (MAGUK) protein family, but in *Drosophila* its homolog polychaetoid localizes at adherens junctions (AJs) and plays essential roles in AJ modulated morphogenetic events in several epithelia (Fanning and Anderson, 2009; Wei and Ellis, 2001; Choi et al., 2011; Jung et al., 2006; Seppa et al., 2008; Manning et al., 2019). The localization and function of ZO-1 in *S. purpuratus* embryo remains to be determined but the expression of its orthologs has been recently reported in the developing excretory organs of various marine invertebrates (Gąsiorowski et al., 2021).

We further found that a set of SJ gene orthologs were not expressed or had very low expression levels prior and during gastrulation and were

associated with the developing gut epithelium in later stages. Amongst those genes were *Sp_lethal giant larva (lgl)*, *Sp_protein 4.1*, and *Spmesh*. Out of the latter genes, *Spmesh* expression was found exclusively in the endodermal gut cells (Figs. 1 and 3C) which is in agreement with its endodermal expression during early development in *Drosophila* (more detailed discussion below; Izumi et al., 2012). On the other hand, *Splgl* was additionally distributed in the apical ectodermal cells and as revealed by scRNAseq, *Sp_protein 4.1* expression was highly elevated in the mesenchymal pigment cells which have immune function (Figs. 1 and 3 A, B; Perillo et al., 2020). *Drosophila* Lgl and its protein 4.1 homolog, coracle (*cora*), are the cytoplasmic components of both pSJs found in the ectodermal epithelia and sSJs residing in the endodermal midgut (Strand et al., 1994; Lamb et al., 1998; Izumi et al., 2012). Lgl is also required for the establishment of cell polarity, cell shape change and growth control within several *Drosophila* epithelia, including midgut, and its importance in the epithelial development has been also suggested for other non-insect invertebrates such as the blood fluke *Schistosoma japonicum* and sea anemone *Nematostella vectensis* (Manfruelli et al., 1996; Bilder et al., 2000; Cao et al., 2014; Salinas-Saavedra et al., 2015, 2018). Loss-of-function mutations in *Drosophila cora* reveal many defects in the epithelial tissue migration and organogenesis during embryonic development, imaginal disc morphogenesis during metamorphosis, and oogenesis in adulthood (Lamb et al., 1998; Ward et al., 2003; Hall and Ward, 2016; Lee et al., 2020; Alhadyian et al., 2021). Although it is difficult to speculate on the significance of *Sp_protein 4.1* expression in the larval pigment cells seen in the current study, it is important to note that *Drosophila* Cora is also a component of the ROS (reactive oxygen species) signalling pathway in the non-epithelial SJ-lacking pericardial cells required to regulate critical processes in the neighboring cardiomyocytes (Lim et al., 2019).

A MAGUK protein discs large (Dlg) is another *Drosophila* pSJ- and sSJ-associated protein that is also required for proper apicobasal polarity and proliferation control in embryonic epithelia (Woods et al., 1996; Bilder et al., 2000). Supported by both in situ hybridization and scRNAseq, we found a gene encoding for Dlg homolog in *S. purpuratus* expressed early and transiently in the blastula skeletogenic PMCs undergoing epithelial-to-mesenchymal transition (EMT) (Figs. 1 and 3D; Katow, 2015). In the later stages, *Spdlg* distribution appeared to be confined to the developing gut epithelium. In the sea urchin embryo, the process of EMT in the PMC formation includes the loss of cell affinity to the epithelium lining apical and basal extracellular matrices and inter-cell adhesion (Katow, 2015). The timing of *Spdlg* expression in the PMCs of *S. purpuratus* blastula seems to suggest its potential involvement during this process. Future investigations will help determine SpDlg function in the EMT but in *Drosophila*, modulation of Dlg activity is required during oogenesis when a cluster of cells, the border cells, delaminate from the follicular epithelium and migrate through the egg chamber (Szafranski and Goode, 2004, 2007).

Lastly, we identified *Sp_neuroglian-like* (*nrg*), a homolog of cell adhesion molecule neuroglian (Nrg) required for pSJ formation in the ectodermal epithelia of *Drosophila* (Genova and Fehon, 2003). The timing and location of *Spnrg* expression in the ecodermal and endodermal gut epithelia was seen similar to that of *Splgl* (Fig. 1) which might suggest their cellular interaction. Interestingly, in adult *Drosophila* midgut, unlike Lgl, Nrg is not a component of sSJs between the major enterocyte cells but its expression is required in the SJ-lacking intestinal stem cells (ISCs) and enteroblasts to regulate ISC proliferation (Resnik-Docampo et al., 2021). To our surprise, *Spnrg* mRNA transcripts were not detected in any cells across all stages by scRNAseq (data not shown).

5. A shared role for mesh in invertebrate intestinal SJ barrier

The presence of proteins homologous to *Drosophila* Mesh in other invertebrates, including sea urchins and *Caenorhabditis elegans*, have been previously identified but their functions in non-insect species have not been studied to date (Izumi et al., 2012). In *Drosophila*, Mesh protein expression is first detected post-gastrulation in the endodermally-derived tissues and by larval stage, Mesh localizes specifically to sSJs found between the epithelial cells of the proventriculus, midgut, and Malpighian (renal) tubules (Izumi et al., 2012). In larval fly midgut, Mesh is required for sSJ formation at the ultrastructural level and for proper junctional localization of other integral sSJ proteins (Izumi et al., 2012, 2016, 2021). Observations made in our study indicate that Mesh is also expressed post-gastrulation in *S. purpuratus* and is restricted to the endodermally-derived gut where it localizes to the SJs residing in the midgut and hindgut epithelia by early pluteus stage (Fig. 4 and Fig. S7). It has been shown that during late gastrulation in a green sea urchin *S. drobachiensis*, the invaginated endodermal gut cells start to form the single-septum anastomosing SJs detected well in pluteus larva and which are different from the straight double-septum SJs that remain between the cells of the ectoderm (Spiegel and Howard, 1983). The timing of expression and subcellular localization of SpMesh revealed in our study, including the cytoplasmic distribution and large aggregates in the gut cells of prism larva and concentration at cell-cell contact regions by 72 hpf (Fig. 4), may further suggest that Mesh plays a role in the assembly of echinoderm anastomosing SJs. It is interesting to note the lack of SpMesh expression in the foregut epithelium of pluteus larva despite its endodermal origin and presumably having the same anastomosing SJs (Annunziata et al., 2014). In *Drosophila*, Mesh is absent in the foregut and the hindgut which have ectodermal pSJs (Izumi et al., 2012). These observations raise the possibility that instead of being restricted to the specific type of SJ, Mesh expression is restricted to the epithelium with a specific function such as digestion in the fly midgut and in the midgut and hindgut of a sea urchin larva (Annunziata et al., 2014).

In the first-instar larval fly midgut, loss of Mesh leads to the paracellular barrier dysfunction with no remarkable defects in the epithelial morphology (Izumi et al., 2012). We extend these observations in the present study and find that *Spmesh*-deficient early sea urchin larvae develop normal guts but have increased seawater-to-body cavity diffusion of 4 kDa FITC-dextran (Fig. 5) which we attribute to increased paracellular leak across the midgut and hindgut. In larval *Drosophila* midgut, the increase in paracellular macromolecule permeability upon loss of Mesh occurs in conjunction with defects in SJ formation at the ultrastructural level, suggesting that Mesh might be one of the components of the septa observed in ultrathin section electron microscopy (Izumi et al., 2012). It is conceivable to suggest a similar role for Mesh in larval sea urchin midgut and hindgut SJs. In addition, it has been demonstrated that insect midgut and other epithelial SJs can display a high selectivity with respect to the size and charge of permeating ions (Fiandra et al., 2006; Pannabecker et al., 1993). Future electrophysiological investigations are warranted to determine if SJs allow the paracellular movement of specific ions across larval sea urchin gut epithelium and if it occurs in Mesh dependent manner.

In adult *Drosophila* midgut, in addition to the maintenance of barrier integrity, Mesh is required for the epithelial organization and homeostasis, including the control of microbiome load (Izumi et al., 2019; Xiao et al., 2017). Since our studies were limited to the early developmental stages of *S. purpuratus* before the larvae started to feed, it is possible that loss of Mesh in the later stages of feeding larvae would lead to more apparent phenotypes. Nevertheless, our results are the first to suggest that as a component of morphologically distinct SJs, Mesh has a similar role in the regulation of invertebrate intestinal barrier.

5.1. Phylogenetic analysis

SJs are one of the most prominent junctions in the epithelia of invertebrates and the genes encoding SJ protein orthologs of best understood *Drosophila* SJ components have been identified in the early branching metazoans (Ganot et al., 2015). These taxa reveal great SJ gene diversification and variability in the range of specific genes and their copies/homologs present, which might underlie subsequent divergence in SJ structure across invertebrate phyla (Ganot et al., 2015;

Jonusaite et al., 2016). We also find multiple copies of *S. purpuratus* genes that belong to the families with members of *Drosophila* SJ components (Fig. S1) but it will require future studies to determine if they are all associated with SJs in the sea urchin, as we have shown here for SpMesh. The lack of molecular and functional investigations of SJs in diverse invertebrate groups hinders our understanding of the bona fide SJ proteins. Importantly, the presence of different set of integral SJ components in *Drosophila* pSJs and sSJs, with the latter containing some proteins found only in insect and/or arthropod species (Yanagihashi et al., 2012; Rouka et al., 2021; Izumi et al., 2021), further suggests that unique yet to be discovered molecules function in other SJ variants, such as those found in echinoderms.

Although vertebrates lack epithelial SJs and instead have evolved TJs as their functional counterparts, a junction structurally similar to SJs, the paranodal SJ, is present in vertebrates in the myelinated nerves between the myelin loops and the axonal membrane at the paranodal interface (Banerjee et al., 2006). Functionally, vertebrate paranodal SJs provide ionic diffusion barrier into the periaxonal space, and serve as a fence to maintain the axonal domains and prevent lateral diffusion of various membrane protein complexes (Boyle et al., 2001; Rios et al., 2003). Vertebrate paranodal SJs also share some molecular components with *Drosophila* pSJs, such as cell-adhesion molecules contactin and neuroglian/neurofascin, suggesting their evolution from ancestral SJs (Banerjee et al., 2006; Harden et al., 2016). It is also interesting to note that although *Drosophila* SJs and vertebrate TJs show striking differences in their respective integral proteins, the cytosolic scaffold components responsible for their assembly and maintenance at the plasma membrane appear to share, in part, similar machineries, such as MAGUK proteins ZO-1 and Dlg, FERM protein cora/protein 4.1, as well as Lgl (Ganot et al., 2015; Harden et al., 2016; Yamanaka and Ohno, 2008). In light of the notion that echinoderms are the epithelial SJ-bearing deuterostomes and sister group of vertebrates, further identification and functional characterization of SJ proteins in echinoderms is of great interest not only in terms of cell biology and physiology, but also the evolution of paracellular barrier regulating junctions in both epithelial and non-epithelial tissues.

5.2. Potential environmental implications

The evidence is convincing that invertebrate SJs show functional plasticity and their permeability is adjusted in response to altered environmental conditions when maintenance of internal milieu is at risk. For example, changes in SJ permeability, which manifests as alterations in SJ morphology and/or SJ protein expression, occur in the ion and water transporting epithelia of freshwater larval insects when they encounter increased environmental salinity (Jonusaite et al., 2017b a,b; Nowghani et al., 2019). Adult *Drosophila* flies have greater tolerance to low temperature stress due to in part reduced gut SJ permeability (MacMillan et al., 2017). Importantly, a recent study on a marine invertebrate, a reef-building coral *Stylophora pistillata*, has reported alterations in its epithelial SJ permeability in response to low seawater pH and changes in temperature which both can have negative effects on coral calcification (Venn et al., 2020). Climate driven ocean changes, including ocean acidification and warming, are projected to have profound effects on the survival and fitness of marine taxa and to make better predictions, it is critical to identify the physiological traits that determine the sensitivity and resilience among species and across specific life cycle stages (Melzner et al., 2009; Kroeker et al., 2013; Przeslawski et al., 2015; Kavousi et al., 2022; Asnicar and Marin, 2022). Functional SJ plasticity in the epithelia that are in direct contact with the sea water such as the ectoderm and the gut of planktonic larval stages might offer the first line of defense against changing oceanic conditions. In the specific case of sea urchin larva, adjustments in SJ permeability properties of these epithelia might contribute to the maintenance of distinct ionic and pH environments in the gut and body cavity. Regulation of ionic and acid-base balance is essential for larval growth, intestinal health, and skeleton formation and these processes are challenged by decrease in seawater pH (Stumpp et al., 2011, 2012, 2013, 2015; Padilla-Gamiño et al., 2013; Dorey et al., 2013; Pan et al., 2015; Lee et al., 2019; Petersen et al., 2021). It has been suggested that the ability to maintain alkaline midgut pH required for digestion may be a key trait underlying the degree and variability of species-specific sensitivity of echinoderm larvae to seawater acidification (Stumpp et al., 2013; 2015; Hu et al., 2017). Recent insect studies have already uncovered the importance of midgut SJ functional plasticity during acclimation to environmental perturbations (MacMillan et al., 2017; Jonusaite et al., 2017b a,b). Therefore, the discovery of Mesh as an integral SJ component in the midgut and hindgut of early *S. purpuratus* larva as well as epithelial expression of other SJ gene orthologs (Fig. 1) provide a strong impetus to consider in the future studies the roles of SJ proteins in mediating homeostatic responses of marine larvae in an era of rapid climate change.

Funding

This work was supported by the Natural Sciences and Engineering Research Council of Canada [Discovery Grant 400230 to AH, postdoctoral fellowship to SJ], the National Institutes of Health (USA) [1R35GM140897 to GMW, 1P20GM119943 to NO], the National Science Foundation (USA) [IOS-1923445 to GMW], Grant-in-Aid for Scientific Research (C) from the Japan Society for the Promotion of Science [15K07048, 19K06650 to YI], and by a Funding Program for Next Generation, World Leading Researchers (NEXT Program) from the Japan Society for the Promotion of Science initiated by the Council for Science and Technology Policy [LS084 to MF].

Declaration of competing interest

None.

Data availability

Data will be made available on request.

Acknowledgments

The authors would like to thank the Van Ray Lab for assistance and use of Western blot equipment and Molecular and Cellular Imaging facility at the University of Guelph.

Appendix A. Supplementary data

Supplementary data to this article can be found online at https://doi.org/10.1016/j.ydbio.2022.12.007.

References

Adonin, L., Drozdov, A., Barlev, N.A., 2021. Sea urchin as a universal model for studies of gene networks. Front. Genet. 11, 627259.
Alhadyian, H., Shoaib, D., Ward, R.E., 2021. Septate junction proteins are required for egg elongation and border cell migration during oogenesis in Drosophila. G3 (Bethesda) 11, jkab127.
Anderson, J.M., Van Itallie, C.M., 2009. Physiology and function of the tight junction. Cold Spring Harbor Perspect. Biol. 1, a002584.
Annunziata, R., Perillo, M., Andrikou, C., Cole, A.G., Martinez, P., Arnone, M.I., 2014. Pattern and process during sea urchin gut morphogenesis: the regulatory landscape. Genesis 52, 251–268.
Arnone, M., Byrne, M., Martínez, P., 2015. Echinodermata. In: Wanninger, A. (Ed.), Evolutionary Developmental Biology of Invertebrates 6: Deuterostomia. Springer-Verlag, Wien, pp. 1–58.
Asnicar, D., Marin, M.G., 2022. Effects of seawater acidification on echinoid adult stage: a review. J. Mar. Sci. Eng. 10, 477.
Banerjee, S., Sousa, A.D., Bhat, M.A., 2006. Organization and function of septate junctions: an evolutionary perspective. Cell Biochem. Biophys. 46, 65–77.
Beyenbach, K.W., Schöne, F., Breitsprecher, L.F., Tiburcy, F., Furuse, M., Izumi, Y., Meyer, H., Jonusaite, S., Rodan, A.R., Paululat, A., 2020. The septate junction protein Tetraspanin 2A is critical to the structure and function of Malpighian tubules in *Drosophila melanogaster*. Am. J. Physiol. Cell Physiol. 318, C1107–C1122.

Bilder, D., Li, M., Perrimon, N., 2000. Cooperative regulation of cell polarity and growth by Drosophila tumor suppressors. Science 289, 113–116.
Boyle, M.E., Berglund, E.O., Murai, K.K., Weber, L., Peles, E., Ranscht, B., 2001. Contactin orchestrates assembly of the septate-like junctions at the paranode in myelinated peripheral nerve. Neuron 30, 385–397.
Brinkman, E.K., Chen, T., Amendola, M., van Steensel, B., 2014. Easy quantitative assessment of genome editing by sequence trace decomposition. Nucleic Acids Res. 42, e168.
Cao, Y., Shi, Y., Qiao, H., Yang, Y., Liu, J., Shi, Y., Lin, J., Zhu, G., Jin, Y., 2014. Distribution of lethal giant larvae (Lgl) protein in the tegument and negative impact of siRNA-based gene silencing on worm surface structure and egg hatching in Schistosoma japonicum. Parasitol. Res. 113, 1–9.
Charrin, S., Jouannet, S., Boucheix, C., Rubinstein, E., 2014. Tetraspanins at a glance. J. Cell Sci. 127, 3641–3648.
Choi, W., Jung, K.C., Nelson, K.S., Bhat, M.A., Beitel, G.J., Peifer, M., Fanning, A.S., 2011. The single drosophila zo-1 protein polychaetoid regulates embryonic morphogenesis in coordination with canoe/afadin and enabled. Mol. Biol. Cell 22, 2010–2030.
Dan-Sohkawa, M., Kaneko, H., Noda, K., 1995. Paracellular, transepithelial permeation of macromolecules in the body wall epithelium of starfish embryos. J. Exp. Zool. 271, 264–272.
Dorey, N., Lançon, P., Thorndyke, M., Dupont, S., 2013. Assessing physiological tipping point of sea urchin larvae exposed to a broad range of pH. Global Change Biol. 19, 3355–3367.
Faivre-Sarrailh, C., Banerjee, S., Li, J., Hortsch, M., Laval, M., Bhat, M.A., 2004. *Drosophila* contactin, a homolog of vertebrate contactin, is required for septate junction organization and paracellular barrier function. Development 131, 4931–4942.
Fanning, A.S., Anderson, J.M., 2009. Zonula occludens-1 and -2 are cytosolic scaffolds that regulate the assembly of cellular junctions. Ann NY Acad Sci 1165, 113–120.
Ferguson, D.P., Dangott, L.J., Lightfoot, J.T., 2014. Lessons learned from vivo-morpholinos: how to avoid vivo-morpholino toxicity. Biotechniques 56, 251–256.
Fiandra, L., Casartelli, M., Giordana, B., 2006. The paracellular pathway in the lepidopteran larval midgut: modulation by intracellular mediators. Comp. Biochem. Physiol. Mol. Integr. Physiol. 144, 464–473.
Foster, S., Oulhen, N., Wessel, G., 2020. A single cell RNA sequencing resource for early sea urchin development. Development 147, dev191528.
Furuse, M., 2010. Molecular basis of the core structure of tight junctions. Cold Spring Harbor Perspect. Biol. 2, a002907.
Ganot, P., Zoccola, D., Tambutté, E., Voolstra, C.R., Aranda, M., Allemand, D., Tambutté, S., 2015. Structural molecular components of septate junctions in cnidarians point to the origin of epithelial junctions in eukaryotes. Mol. Biol. Evol. 32, 44–62.
Gąsiorowski, L., Andrikou, C., Janssen, R., Bump, P., Budd, G.E., Lowe, C.J., Hejnol, A., 2021. Molecular evidence for a single origin of ultrafiltration-based excretory organs. Curr. Biol. 31, 3629–3638.e2.
Genova, J.L., Fehon, R.G., 2003. Neuroglian, gliotactin, and the Na^+/K^+ ATPase are essential for septate junction function in *Drosophila*. J. Cell Biol. 161, 979–989.
Green, C.R., 1981. Fixation-induced intramembrane particle movement demonstrated in freeze-fracture replicas of a new type of septate junction in echinoderm epithelia. J Ultrastruct Res 75, 11–22.
Green, C.R., Bergquist, P.R., 1982. Phylogenetic relationships within the invertebrates in relation to the structure of septate junctions and the development of 'occluding' junctional types. J. Cell Sci. 53, 279–305.
Green, C.R., Bergquist, P.R., Bullivant, S., 1979. An anastomosing septate junction in endothelial cells of the phylum echinodermata. J. Ultrastruct. Res. 68, 72–80.
Hall, S., Ward, R.E.I.V., 2016. Septate junction proteins play essential roles in morphogenesis throughout embryonic development in *Drosophila*. G3 (Bethesda) 6, 2375–2384.
Harden, N., Wang, S.J., Krieger, C., 2016. Making the connection - shared molecular machinery and evolutionary links underlie the formation and plasticity of occluding junctions and synapse. J. Cell Sci. 129, 3067–3076.
Heyland, A., Hodin, J., Bishop, C., 2014. Manipulation of developing juvenile structures in purple sea urchins (*Strongylocentrotus purpuratus*) by morpholino injection into late stage larvae. PLoS One 9, e113866.
Hu, M., et al., 2017. Variability in larval gut pH regulation defines sensitivity to ocean acidification in six species of the Ambulacraria superphylum. Proc. Biol. Sci. 284 (1864), 20171066.
Itza, E.M., Mozingo, N.M., 2005. Septate junctions mediate the barrier to paracellular permeability in sea urchin embryos. Zygote 13, 255–264.
Izumi, Y., Furuse, M., 2014. Molecular organization and function of invertebrate occluding junctions. Semin. Cell Dev. Biol. 36, 186–193.
Izumi, Y., Yanagihashi, Y., Furuse, M., 2012. A novel protein complex, Mesh-Ssk, is required for septate junction formation in the *Drosophila* midgut. J. Cell Sci. 125, 4923–4933.
Izumi, Y., Motoishi, M., Furuse, K., Furuse, M., 2016. A tetraspanin regulates septate junction formation in *Drosophila* midgut. J. Cell Sci. 129, 1155–1164.
Izumi, Y., Furuse, K., Furuse, M., 2019. Septate junctions regulate gut homeostasis through regulation of stem cell proliferation and enterocyte behavior in *Drosophila*. J. Cell Sci. 132, jcs232108.
Izumi, Y., Furuse, K., Furuse, M., 2021. The novel membrane protein Hoka regulates septate junction organization and stem cell homeostasis in the Drosophila gut. J. Cell Sci. 134, jcs257022.
Jonusaite, S., Rodan, A.R., 2021. Molecular basis for epithelial morphogenesis and ion transport in the Malpighian tubule. Curr. Opin. Insect Sci. 47, 7–11.
Jonusaite, S., Donini, A., Kelly, S.P., 2016. Occluding junctions of invertebrate epithelia. J. Comp. Physiol. B 186, 17–43.
Jonusaite, S., Donini, A., Kelly, S.P., 2017a. Salinity alters snakeskin and mesh transcript abundance and permeability in midgut and Malpighian tubules of larval mosquito, *Aedes aegypti*. Comp. Biochem. Physiol. Mol. Integr. Physiol. 205, 58–67.
Jonusaite, S., Kelly, S.P., Donini, A., 2017b. Identification of the septate junction protein gliotactin in the mosquito *Aedes aegypti*: evidence for a role in increased paracellular permeability in larvae. J. Exp. Biol. 220, 2354–2363.
Jonusaite, S., Beyenbach, K.W., Meyer, H., Paululat, A., Izumi, Y., Furuse, M., Rodan, A.R., 2020. The septate junction protein Mesh is required for epithelial morphogenesis, ion transport, and paracellular permeability in the *Drosophila* Malpighian tubule. Am. J. Physiol. Cell Physiol. 318, C675–C694.
Jung, A.C., Ribeiro, C., Michaut, L., Certa, U., Affolter, M., 2006. Polychaetoid/zo-1 is required for cell specification and rearrangement during drosophila tracheal morphogenesis. Curr. Biol. 16, 1224–1231.
Katow, H., 2015. Mechanisms of the epithelial-to-mesenchymal transition in sea urchin embryos. Tissue Barriers 3, e1059004.
Kavousi, J., Roussel, S., Martin, S., Gaillard, F., Badou, A., Di Poi, C., Huchette, S., Dubois, P., Auzoux-Bordenave, S., 2022. Combined effects of ocean warming and acidification on the larval stages of the European abalone *Haliotis tuberculata*. Mar. Pollut. Bull. 175, 113131.
Kolosov, D., Jonusaite, S., Donini, A., Kelly, S.P., O'Donnell, M.J., 2019. Septate junction in the distal ileac plexus of larval lepidopteran *Trichoplusia ni*: alterations in paracellular permeability during ion transport reversal. J. Exp. Biol. 222, jeb204750.
Kroeker, K.J., Kordas, R.L., Crim, R., Hendriks, I.E., Ramajo, L., Singh, G.S., Duarte, C.M., Gattuso, J.-P., 2013. Impacts of ocean acidification on marine organisms: quantifying sensitivities and interaction with warming. Global Change Biol. 19, 1884–1896.
Krupinski, T., Beitel, G.J., 2009. Unexpected roles of the Na-K-ATPase and other ion transporters in cell junctions and tubulogenesis. Physiology 24, 192–201.
Lamb, R.S., Ward, R.E., Schweizer, L., Fehon, R.G., 1998. *Drosophila* coracle, a member of the protein 4.1 superfamily, has essential structural functions in the septate junctions and developmental functions in embryonic and adult epithelial cells. Mol. Biol. Cell 9, 3505–3519.
Laprise, P., Lau, K.M., Harris, K.P., Silva-Gagliardi, N.F., Paul, S.M., Beronja, S., Beitel, G.J., McGlade, C.J., Tepass, U., 2009. Yurt, Coracle, Neurexin IV and the Na^+,K^+-ATPase form a novel group of epithelial polarity proteins. Nature 459, 1141–1145.
Lee, H.G., Stumpp, M., Yan, J.J., Tseng, Y.C., Heinzel, S., Hu, M.Y., 2019. Tipping points of gastric pH regulation and energetics in the sea urchin larva exposed to CO_2-induced seawater acidification. Comp. Biochem. Physiol. Mol. Integr. Physiol. 234, 87–97.
Lee, S.R., Hong, S.T., Choi, K.W., 2020. Regulation of epithelial integrity and organ growth by Tctp and Coracle in *Drosophila*. PLoS Genet. 16, e1008885.
Lim, H.Y., Bao, H., Liu, Y., Wang, W., 2019. Select septate junction proteins direct ROS-mediated paracrine regulation of *Drosophila* cardiac function. Cell Rep. 28, 1455–1470 e1454.
Lin, C.Y., Oulhen, N., Wessel, G., Su, Y.H., 2019. CRISPR/Cas9-mediated genome editing in sea urchins. Methods Cell Biol. 151, 305–321.
Love, A.C., Andrews, M.E., Raff, R.A., 2007. Gene expression patterns in a novel animal appendage: the sea urchin pluteus arm. Evol. Dev. 9, 51–68.
MacMillan, H.A., Yerushalmi, G., Jonusaite, S., Kelly, S.P., Donini, A., 2017. Thermal acclimation mitigates paracellular leak from the *Drosophila* gut. Sci. Rep. 7, 8807.
Manfruelli, P., Arquier, N., Hanratty, W.P., Sémériva, M., 1996. The tumor suppressor gene, lethal(2)giant larvae (1(2)g1), is required for cell shape change of epithelial cells during *Drosophila* development. Development 122, 2283–2294.
Manning, L.A., Perez-Vale, K.Z., Schaefer, K.N., Sewell, M.T., Peifer, M., 2019. The Drosophila Afadin and ZO-1 homologues Canoe and Polychaetoid act in parallel to maintain epithelial integrity when challenged by adherens junction remodeling. Mol. Biol. Cell 30, 1938–1960.
McClay, D.R., 2011. Evolutionary crossroads in developmental biology: sea urchins. Development 138, 2639–2648.
Melzner, F., Gutowska, M.A., Langenbuch, M., Dupont, S., Lucassen, M., Thorndyke, M.C., Bleich, M., Pörtner, H.O., 2009. Physiological basis for high CO_2 tolerance in marine ectothermic animals: pre-adaptation through lifestyle and ontogeny? Biogeosciences 6, 2313–2331.
Nowghani, F., Chen, C.C., Jonusaite, S., Watson-Leung, T., Kelly, S.P., Donini, A., 2019. Impact of salt-contaminated freshwater on osmoregulation and tracheal gill function in nymphs of the mayfly *Hexagenia rigida*. Aquat. Toxicol. 211, 92–104.
Oulhen, N., Wessel, G.M., 2016. Albinism as a visual, in vivo guide for CRISPR/Cas9 functionality in the sea urchin embryo. Mol. Reprod. Dev. 83, 1046–1047.
Padilla-Gamiño, J.L., Kelly, M.W., Evans, T.G., Hofmann, G.E., 2013. Temperature and CO_2 additively regulate physiology, morphology and genomic responses of larval sea urchins, *Strongylocentrotus purpuratus*. Proc. Biol. Sci. 280, 20130155.
Pan, T.C., Applebaum, S.L., Manahan, D.T., 2015. Experimental ocean acidification alters the allocation of metabolic energy. Proc. Natl. Acad. Sci. U. S. A. 112, 4696–4701.
Pannabecker, T.L., Hayest, T.K., Beyenbach, K.W., 1993. Regulation of epithelial shunt conductance by the peptide leucokinin. J. Membr. Biol. 132, 63–76.
Paul, S.M., Ternet, M., Salvaterra, P.M., Beitel, G.J., 2003. The Na^+/K^+ ATPase is required for septate junction function and epithelial tube-size control in the *Drosophila* tracheal system. Development 130, 4963–4974.
Paul, S.M., Palladino, M.J., Beitel, G.J., 2007. A pump-independent function of the Na,K-ATPase is required for epithelial junction function and tracheal tube size control. Development 134, 147–155.
Perillo, M., Oulhen, N., Foster, S., Spurrell, M., Calestani, C., Wessel, G., 2020. Regulation of dynamic pigment cell states at single-cell resolution. Elife 9, e60388.
Petersen, I., Chang, W.W.J., Hu, M.Y., 2021. Na^+/H^+ exchangers differentially contribute to midgut fluid sodium and proton concentration in the sea urchin larva. J. Exp. Biol. 224, jeb240705.

Przeslawski, R., Byrne, M., Mellin, C., 2015. A review and meta-analysis of the effects of multiple abiotic stressors on marine embryos and larvae. Global Change Biol. 21, 2122–2140.

Rajasekaran, S.A., Palmer, L.G., Moon, S.Y., Peralta Soler, A., Apodaca, G.L., Harper, J.F., Zheng, Y., Rajasekaran, A.K., 2001. Na,K-ATPase activity is required for formation of tight junctions, desmosomes, and induction of polarity in epithelial cells. Mol. Biol. Cell 12, 3717–3732.

Rajasekaran, S.A., Barwe, S.P., Gopal, J., Ryazantsev, S., Schneeberger, E.E., Rajasekaran, A.K., 2007. Na-K-ATPase regulates tight junction permeability through occludin phosphorylation in pancreatic epithelial cells. Am. J. Physiol. Gastrointest. Liver Physiol. 292, G124–G133.

Resnik-Docampo, M., Cunningham, K.M., Ruvalcaba, S.M., Choi, C., Sauer, V., Jones, D.L., 2021. Neuroglian regulates Drosophila intestinal stem cell proliferation through enhanced signaling via the epidermal growth factor receptor. Stem Cell Rep. 16, 1584–1597.

Rice, C., De, O., Alhadyian, H., Hall, S., Ward, R.E., 2021. Expanding the junction: new insights into non-occluding roles for septate junction proteins during development. J. Dev. Biol. 9, 11.

Rios, J.C., Rubin, M., St Martin, M., Downey, R.T., Einheber, S., Rosenbluth, J., Levinson, S.R., Bhat, M., Salzer, J.L., 2003. Paranodal interactions regulate expression of sodium channel subtypes and provide a diffusion barrier for the node of Ranvier. J. Neurosci. 23, 7001–7011.

Rouka, E., Gourgoulianni, N., Lüpold, S., Hatzoglou, C., Gourgoulianis, K., Blanckenhorn, W.U., Zarogiannis, S.G., 2021. The Drosophila septate junctions beyond barrier function: review of the literature, prediction of human orthologs of the SJ-related proteins and identification of protein domain families. Acta Physiol. 231, e13527.

Salinas-Saavedra, M., Stephenson, T.Q., Dunn, C.W., Martindale, M.Q., 2015. Par system components are asymmetrically localized in ectodermal epithelia, but not during early development in the sea anemone *Nematostella vectensis*. EvoDevo 6, 20.

Salinas-Saavedra, M., Rock, A.Q., Martindale, M.Q., 2018. Germ layer-specific regulation of cell polarity and adhesion gives insight into the evolution of mesoderm. Elife 7, e36740.

Seppa, M.J., Johnson, R.I., Bao, S., Cagan, R.L., 2008. Polychaetoid controls patterning by modulating adhesion in the drosophila pupal retina. Dev. Biol. 318, 1–16.

Sheets, J.N., Patrick, M.E., Egland, K.A., 2020. SUSD2 expression correlates with decreased metastasis and increased survival in a high-grade serous ovarian cancer xenograft murine model. Oncotarget 11, 2290–2301.

Spiegel, E., Howard, L., 1983. Development of cell junctions in sea urchin embryos. J. Cell Sci. 62, 27–48.

Strand, D., Raska, I., Mechler, B.M., 1994. The Drosophila lethal(2)giant larvae tumor suppressor protein is a component of the cytoskeleton. J. Cell Biol. 127, 1345–1360.

Stumpp, M., Wren, J., Melzner, F., Thorndyke, M.C., Dupont, S., 2011. CO_2 induced seawater acidification impacts sea urchin larval development I: elevated metabolic rates decrease scope for growth and induce developmental delay. Comp. Biochem. Physiol. A 160, 320–330.

Stumpp, M., Hu, M.Y., Melzner, F., Gutowska, M.A., Dorey, N., Himmerkus, N., Holtmann, W.C., Dupont, S.T., Thorndyke, M.C., Bleich, M., 2012. Acidified seawater impacts sea urchin larvae pH regulatory systems relevant for calcification. Proc. Natl. Acad. Sci. U. S. A. 109, 18192–18197.

Stumpp, M., Hu, M.Y., Casties, I., Saborowski, R., Bleich, M., Melzner, F., Dupont, S., 2013. Digestion in sea urchin larvae impaired under ocean acidification. Nat. Clim. Change 3, 1044–1049.

Stumpp, M., Hu, M.Y., Tseng, Y.C., Guh, Y.J., Chen, Y.C., Yu, J.K., Su, Y.H., Hwang, P.P., 2015. Evolution of extreme stomach pH in bilateria inferred from gastric alkalization mechanisms in basal deuterostomes. Sci. Rep. 5, 10421.

Szafranski, P., Goode, S., 2004. A Fasciclin 2 morphogenetic switch organizes epithelial cell cluster polarity and motility. Development 131, 2023–2036.

Szafranski, P., Goode, S., 2007. Basolateral junctions are sufficient to suppress epithelial invasion during Drosophila oogenesis. Dev. Dynam. 236, 364–373.

Tiklová, K., Senti, K.-A., Wang, S., Gräslund, A., Samakovlis, C., 2010. Epithelial septate junction assembly relies on melanotransferrin iron binding and endocytosis in *Drosophila*. Nat. Cell Biol. 12, 1071–1077.

Vagin, O., Dada, L.A., Tokhtaeva, E., Sachs, G., 2012. The Na-K-ATPase $\alpha_1\beta_1$ heterodimer as a cell adhesion molecule in epithelia. Am. J. Physiol. Cell Physiol. 302, C1271–C1281.

Venn, A.A., Bernardet, C., Chabenat, A., Tambutté, E., Tambutté, S., 2020. Paracellular transport to the coral calcifying medium: effects of environmental parameters. J. Exp. Biol. 223, jeb227074.

Ward, R.E., Evans, J., Thummel, C.S., 2003. Genetic modifier screens in *Drosophila* demonstrate a role for Rho1 signaling in ecdysone-triggered imaginal disc morphogenesis. Genetics 165, 1397–1415.

Wei, X., Ellis, H.M., 2001. Localization of the drosophila maguk protein polychaetoid is controlled by alternative splicing. Mech. Dev. 100, 217–231.

Woods, D.F., Hough, C., Peel, D., Callaini, G., Bryant, P.J., 1996. Dlg protein is required for junction structure, cell polarity, and proliferation control in *Drosophila* epithelia. J. Cell Biol. 134, 1469–1482.

Xiao, X., Yang, L., Pang, X., Zhang, R., Zhu, Y., Wang, P., Gao, G., Cheng, G., 2017. A Mesh-Duox pathway regulates homeostasis in the insect gut. Nat. Microbiol. 2, 17020.

Xu, C., Tang, H.W., Hung, R.J., Hu, Y., Ni, X., Housden, B.E., Perrimon, N., 2019. The septate junction protein Tsp2A restricts intestinal stem cell activity via endocytic regulation of aPKC and Hippo signaling. Cell Rep. 26, 670–688.

Yamanaka, T., Ohno, S., 2008. Role of Lgl/Dlg/Scribble in the regulation of epithelial junction, polarity and growth. Front. Biosci. 13, 6693–6707.

Yanagihashi, Y., Usui, T., Izumi, Y., Yonemura, S., Sumida, M., Tsukita, S., Uemura, T., Furuse, M., 2012. Snakeskin, a membrane protein associated with smooth septate junctions, is required for intestinal barrier function in *Drosophila*. J. Cell Sci. 125, 1980–1990.

Zeng, X., Singh, S.R., Hou, D., Hou, S.X., 2010. Tumor suppressors Sav/Scrib and oncogene Ras regulate stem-cell transformation in adult Drosophila malpighian tubules. J. Cell. Physiol. 224, 766–774.